This is the author's final, peer-reviewed manuscript as accepted for publication (AAM). The version presented here may differ from the published version, or version of record, available through the publisher's website. This version does not track changes, errata, or withdrawals on the publisher's site.

Kinetic Monte Carlo modeling of oxide thin film growth

John A. Purton, Alin M. Elena and G. Teobaldi

Published version information

Citation: JA Purton, AM Elena and G Teobaldi. 'Kinetic Monte Carlo modeling of oxide thin film growth'. J Chem Phys (2022).

DOI: 10.1063/5.0089043

This article may be downloaded for personal use only. Any other use requires prior permission of the author and AIP Publishing. This article appeared as cited above and may be found at DOI above.

This version is made available in accordance with publisher policies. Please cite only the published version using the reference above. This is the citation assigned by the publisher at the time of issuing the AAM. Please check the publisher's website for any updates.

This item was retrieved from **ePubs**, the Open Access archive of the Science and Technology Facilities Council, UK. Please contact epublications@stfc.ac.uk or go to http://epubs.stfc.ac.uk/ for further information and policies.

The Journal of Chemical Physics

Kinetic Monte Carlo modeling of oxide thin film growth

Accepted Manuscript: This article has been accepted for publication and undergone full peer review but has not been through the copyediting, typesetting, pagination, and proofreading process, which may lead to differences between this version and the Version of Record.

Cite as: J. Chem. Phys. (in press) (2022); https://doi.org/10.1063/5.0089043
Submitted: 22 February 2022 • Accepted: 16 May 2022 • Accepted Manuscript Online: 16 May 2022

John A Purton, Alin M. Elena and Gilberto Teobaldi

View Online Export Citation CrossMark

ARTICLES YOU MAY BE INTERESTED IN

Dielectric Constant of Aqueous Solutions of Proteins and Organic Polymers from Molecular Dynamics Simulations
The Journal of Chemical Physics (2022); https://doi.org/10.1063/5.0089397

Adsorption of C2-C5 alcohols on ice. A grand canonical Monte Carlo simulation study
The Journal of Chemical Physics (2022); https://doi.org/10.1063/5.0096013

Lock-in Amplifiers
up to 600 MHz
Zurich Instruments
Watch

AIP Publishing

J. Chem. Phys. (in press) (2022); https://doi.org/10.1063/5.0089043

© 2022 Author(s).

Kinetic Monte Carlo modeling of oxide thin film growth

John A. Purton[a,*], Alin M. Elena [a] and G. Teobaldi[b,c]

a. Scientific Computing Department, STFC-UKRI, Daresbury Laboratory, Keckwick Lane, Warrington, WA4 4AD, UK. Email: john.purton@stfc.ac.uk
b. Scientific Computing Department, STFC-UKRI, Rutherford Appleton Laboratory, Didcot, OX11 0QX, UK
c. School of Chemistry, University of Southampton, Highfield, Southampton SO17 1BJ , UK

Abstract

In spite of the increasing interest in and application of ultrathin film oxide oxides in commercial devices, the understanding of the mechanisms that control the growth of these films at the atomic scale remains limited and scarce. This limited understanding prevents the rational design of novel solutions based on precise control of the structure and properties of ultrathin films. Such a limited understanding stems in no minor part from the fact that most of the available modeling methods are unable to access and robustly sample the nanosecond to second time-scales required to simulate both atomic deposition and surface reorganization at ultrathin films. To contribute to this knowledge gap, here we have combined molecular dynamics and adaptive Kinetic Monte Carlo simulation to study the deposition and growth of oxide materials over an extended timescale of up to approximately 0.5 milliseconds. In our pilot studies we have examined the growth of binary oxide thin films on oxide substrates. We have investigated three scenarios (i) the lattice parameter of both the substrate and thin film are identical (ii) the lattice parameter of the thin film is smaller than the substrate and (iii) the lattice parameter is greater than the substrate. Our calculations allow for the diffusion of ions between deposition events and the identification of growth mechanisms in oxide thin films. We make a detailed comparison with previous calculations. Our results are in good agreement with available experimental results and demonstrate important limitations in former calculations, which fail to sample phase space correctly at the temperatures of interest (typically 300K to 1000K) with self-evident limitations for the representative modeling of thin films growth. We believe the present pilot study and proposed combined methodology open up for extended computational support in the understanding and design of ultrathin film growth conditions tailored to specific applications.

Introduction

Metal-oxide have a wide range of useful properties (being thermoelectrics, ferroelectrics, ion conductors, ferromagnetics, colossal magneto-resistant materials, superconductors, piezoelectrics)[1,2,3] and are thus candidate materials for uses as diverse as energy conversion processes, catalysts and sensors as well as memory applications. The manufacture of devices often demands the ability to exercise precise control over the growth of thin films on a host substrate. Indeed, atomic level definition may be required for applications such as supported superconductors, magnetic, optical and electronic devices. Using techniques such as molecular beam epitaxy (MBE), chemical vapor deposition (CVD) and pulsed laser deposition (PLD), it is possible to produce phases that are very different from those found in the bulk, leading to new nanoscale materials and devices. However, there are significant unsolved experimental challenges in **simultaneous** time- and atomically resolved characterization of “thin-film” phases and their interfaces. The usually limited similarities between bulk and ultrathin film properties of a given materials readily define a vital role for computer simulations in both interpreting the experimental data (such as reflection high-energy electron diffraction, grazing incidence X-ray diffraction transmission electron microscopy results) and uncovering the factors that dominate the resultant film morphology. Moreover, the chemical and physical properties of thin films can change dramatically when supported on a substrate, thus making it essential to understand the mechanism of thin film growth and the importance of the substrate influence on the thin film.

Despite the technological importance of ultra-thin ionic materials, few detailed simulations of the growth of such films exist. Most of these either tried to obtain plausible film structures without attempting a detailed model of the growth, relying on structures obtained using energy minimization, or used classical molecular dynamics simulations with unrealistic timescales (i.e. nanosecond simulations are too short to allow for diffusion of the ions at the surface) and/or very high temperatures.[4,5,6] Notable exceptions include the calculations in references 7 and 8, which employ a computationally demanding adaptive Kinetic Monte Carlo (KMC) approach.[9] In these calculations one or more monolayers of atoms were simultaneously deposited on the surface to achieve high growth rates similar to those in experiments. Recent advances in the speed of computers has allowed us to iteratively deposit small number of ions (equivalent to 7% of a monolayer) and study the re-organization of these ions to form surface structures (see discussion below).

For atomistic simulations to provide detailed information on the structure of interfaces it is essential that they reflect the temperatures and timescales relevant for the process under study. For thin-film growth, deposition temperatures are usually in the 300 to 1000 K range (this depends on many factors such as the technique and chemical components) and the atomistic processes underpinning the film growth and surface re-organization are understood to happen in nanoseconds to seconds time-scales. Towards fulfilment of these conditions in the simulations, we present an approximate method for the multiscale modeling of thin film growth that allows for both the deposition of ions and their subsequent re-organization at the surface. We examine the growth of the binary oxide films (MgO, CaO and SrO) on two substrates as a pilot study for our off-lattice kinetic Monte Carlo method. The substrates employed are MgO and BaO since these provide examples where the substrate and thin film have identical lattice spacing and where the thin film and substrate have a large degree of lattice mismatch. We have also chosen these compounds as Sayle and Watson have studied the binary oxide interfaces using a molecular dynamics amorphization and recrystallization strategy, while Allan *et al.* have employed lattice energy minimization to investigate similar interfaces.[10,11] The amorphization and recrystallization technique involves forcing the overlying material to undergo, under dynamical simulation, a controlled amorphization at an elevated temperature. Subsequently a molecular dynamics simulation on this amorphized thin film results in its recrystallization and the evolution of structural features. Our simulation technique employs the same potential model as the above calculations, thus allowing a meaningful comparison of the results. We demonstrate the variation in modes of thin film growth depending on the difference in lattice parameters of the thin film and substrate.

Computational Methods

Our objective is to study the growth of oxide thin films that are formed in experiments such as pulsed laser deposition (PLD). In PLD a laser is used to vaporize a target material and the atoms/ions are then deposited on to a substrate. The growth of a thin film using PLD can be envisaged as two distinct stages. The first is the deposition of ions on to the surface and the second the reorganization of these atoms/ions on the surface often to form a crystalline material. The former process is fast and can be modelled using traditional Monte Carlo (MC) and molecular dynamics (MD) techniques. Unfortunately, the second process is slow (approximately nanoseconds to seconds depending on the temperature and the size of the diffusion barrier)[12,13,14,15] and MD is not capable of accessing the time scales required for the systems we are interested in. It is thus necessary to use an alternate technique such as KMC. Each simulation of fixed composition can be broken down to two components: an initial MC/MD phase followed by a second KMC phase. Thin film growth is modelled by repeatedly inserting additional ions to the simulation cell and performing combined MC/MD/KMC calculations. All of our simulations were undertaken at 300 K, the regime where the diffusion of ions is slow.

The initial phase of a deposition event is to place the ions in a suitable position chosen at random yet without unphysically short inter-ion distances. This was accomplished using the MC engine DL_MONTE.[16] As the MC often places ions within the vacuum region, a short molecular dynamics calculation, using the DL_POLY package,[17] was employed to allow these ions to adjust their positions and adsorb on the surface of the deposition substrate. At each deposition step 20 divalent cations (e.g. Mg^{2+}, Ba^{2+}) and 20 O^{2-} anions were added to the simulation cell. The MD simulations were run for 50,000 steps using a time step of 1.0 femtoseconds. This procedure was found to produce a “sensible” starting point for the adaptive kinetic Monte Carlo simulations (*i.e.* all the ions are in contact with the surface and the bond lengths are similar to those of the bulk materials) and the resulting configurations were fed into the KMC as described below.

We now turn our attention to describing the details of the KMC phase of the simulation. KMC exploits stochastic algorithms to explore rare events and coarse grain the time evolution of the model system.[18,19,20] In our calculations the transition states are considered as thermally activated diffusional hops and are governed by an Arrhenius equation:

$$r_D = D_0 \exp\left(-\frac{Q}{kT}\right) \qquad [1]$$

where r_D is the rate of an event, D_0 is an exponential pre-factor, Q is the activation energy of the hop, k is Boltzmann's constant and T the temperature. We assume that the exponential pre-factor D_0 represents the attempt frequency for an atom hopping from basin 1 to basin 2. We have employed a value of 10^{13} s^{-1}, which has been determined as a good approximation for oxide materials.[21] In our simulations an event is either a cation or an anion diffusional hop and the state of the model system is evolved by choosing one event stochastically, according to the rate of the events using the following equation:

$$\sum_{i=1}^{m-1} r_i \leq \rho_1 \sum_{j=1}^{N} r_j < \sum_{k=1}^{m} r_k \qquad [2]$$

where m is the index of the chosen event and N is the total number of possible events. Summation indices i, j, and k denote the individual events, thus r_i is the rate of the event i. ρ_i is a random number evenly distributed over the range [0, 1]. This ensures that faster events have a greater probability of being chosen than slower events. Once an event is chosen, the surface is modified to enact the diffusion event. The simulation time is then advanced by

$$\Delta t = -\frac{ln\rho_2}{\sum_{i=1}^{N} r_i} \qquad [3]$$

In equation 3, t is the elapsed time and ρ_2 is a random number evenly distributed over the range [0, 1].

The list of events can be pre-determined or calculated on-the-fly. A pre-determined list requires less computation. However, for thin film growth, prior knowledge of the structure and thus activation energies is not possible and it is necessary to calculate these on-the-fly. Calculation of activation energies requires a method to search for and determine saddle points without input from the user. It is possible to do this with techniques such as molecular dynamics,[22] the dimer method [23] and activation relaxation technique.[24] We have adopted the molecular dynamics approach and summarize the computational approach below.

At each step a NVT ensemble MD run was performed whilst monitoring the displacement of the ions. When an ion(s) was found to have moved more than a given distance (the cation-oxygen distance of the thin film oxide) the MD simulation was paused and the positions adjusted until the forces on the ions were less than 0.001 eV/Å using the FIRE method.[25] The location of the ions was then re-analyzed. If they were found to have fallen back into the original basin the MD simulation was re-started. However, if they relaxed into a new basin the MD run was halted and the activation barrier and energy determined using the Nudged Elastic Band method.[26,27] The NEB calculated activation energies, Q, are employed within the KMC simulation via equations 1-3. By combining MD and NEB it is possible to calculate the activation energies of both single and multiple particle jumps. Approximately 80% of the computational time is taken up in the MD simulation and the efficiency of the molecular dynamics step depends on the frequency of ions moving from one basin to the next and may take a significant number of timesteps. To overcome this problem, we have accelerated the MD using the approach of Hamelberg *et al*.[28] In addition, we collected 100 events per KMC iteration. Fortunately, each event can be evaluated independently and we employed between 24 and 48 concurrent MD simulations (each is initiated with a different set of random velocities). The diffusion of the ions was studied using the KMC simulation for one microsecond and then a further deposition event was initiated, and the process restarted. We have neither employed recycling of activation energies nor used a catalogue of possible events (*i.e.* each activation energy is from a new event).

We would like to emphasize that once relaxation is included in the KMC simulation, it requires the energy and forces to be evaluated. As in previous calculations for the same systems as considered here, we have employed the ionic model.[4,10] The interaction energy between two particles *i* and *j* is written as:

$$U_{ij} = Aexp\frac{-r_{ij}}{\rho} - \frac{C}{r_{ij}^6} + \frac{q_i q_j}{r_{ij}}$$

The first two terms on the right-hand side together form an interatomic potential of the Buckingham form. For all calculations presented in this paper we used the potential set developed by Lewis and Catlow.[29] However, we used the rigid ion formalism and do not allow the ions to polarize (i.e. shells were not included as they adversely affect the computational efficiency and the parameterization is poor, if not non-existent, at the transition state). The final term is the Coulomb interaction and is evaluated using the Ewald technique.[30]

Results

In our pilot studies of thin film growth, we have limited our attention to interfaces with rock salt structure as there are several previous publications that have focused on these systems using MD and energy minimization techniques. In all our simulations the substrate was the (001) facet using the slab approximation and each substrate layer consisted of 576 ions. A total of twenty layers of substrate were used in all simulations, but only the uppermost eight layers were allowed to relax. A constant surface (or interfacial) area was assumed and the lattice parameter of the substrate was imposed on the thin film. We have undertaken simulations in which the lattice parameter of the thin film is i) identical, ii) less than and iii) greater than that of the growth-substrate. More specifically, the systems we considered for each class are i) the growth of MgO on a MgO(001), ii) MgO and CaO on the BaO(001) surface, and iii) CaO and SrO on the MgO(001) surface. Throughout this paper the term monolayer is used to refer to the number of ions on the surface and 576 ions will be regarded as a monolayer regardless of whether a single uniform layer is produced or not. In addition, a maximum of three monolayers of ions were deposited on each substrate.

MgO growth on a MgO(001) substrate.

We initially examine the deposition and growth of Mg^{2+} and O^{2-} ions on a MgO(001) substrate, where there is no cation or anion mismatch. Initially, any ions deposited on terraces diffuse to the principal surface plane as the Mg^{2+}-O^{2-} interaction and the ions attempt to maximize the number of nearest neighbors. The Mg^{2+} and O^{2-} ions diffuse on the surface predominantly hopping from a position above their counter ion to an adjacent site. The activation energy for the diffusion of isolated Mg^{2+} and O^{2-} ions is 0.59 eV, which is consistent with the values of 0.3/0.38 and 0.88 eV derived from *ab initio* calculations.[31,32] The simulations in this study demonstrate the formation of small MgO islands containing [100] edges (Figure 1a). Similar islands have been observed for BaO growth on BaO in kinetic Monte Carlo calculations for which the activation energies were determined using temperature accelerated dynamics.[33] Antoshchenkova *et. al.*[34] have studied the growth of MgO on a MgO(001) substrate using an on-lattice, list based KMC method. These authors define four types of "move" (i) rotation of Mg^{2+} around O^{2-}, (ii) rotation of O^{2-} around Mg^{2+}, (iii) exchange of Mg with the surface Mg, and (iv) simultaneous jump of two ions. However, in addition to translation of ions we also frequently observe diffusion events in which there is a translation of several ions, which is not included within the kinetic Monte Carlo approach in Ref. 34. These deviations illustrate exemplarily the difficulties (and risks) in arbitrarily predicting complex moves, such as those observed in Figure 2, in non-adaptive, list-based KMC approaches. In Figure 3, we have plotted the number of particles involved in a single move vs. the activation energy and the total distance of the atoms displaced during a single diffusion event (this is the sum of the distances moved for the atoms that have been displaced more than 1.0 Å) against the activation energy. The data shows that there are many complex multi-atom moves including translations of groups of atoms (approximately 24% of the AKMC events are for the displacement of at least two atoms). Moreover, the total distance moved by atoms within a single diffusion event is unrelated to the activation energy. This, combined with the long-range nature of the Coulomb interactions, prevents the use of recycling schemes. Moreover, when the monolayer coverage is low, we do not observe any exchange of ions between the thin film and substrate since the activation energy for this diffusion mechanism (approximately 1.8 eV) is significantly greater than that for the simple hop (0.59 eV).[31] As more ions are deposited on the substrate the size of the islands increases before fully wetting the substrate as observed in Figure 1b. When the monolayer is almost complete, it is energetically favorable for the Mg^{2+} and O^{2-} ions to move out of the *thin film* plane onto the surface (the frequency of these events is approximately 0.1%) and then diffuse across the top layer to annihilate any imperfections in the thin film (Figure 1b), thus reducing any residual strain. This change in diffusion behavior is difficult to capture by list-based kinetic Monte Carlo. The layer-by-layer growth observed is in agreement with previous experiments and KMC calculations as further deposition of ions results in their diffusion to fill into the forming monolayer and the process restarts.[35]

(a)

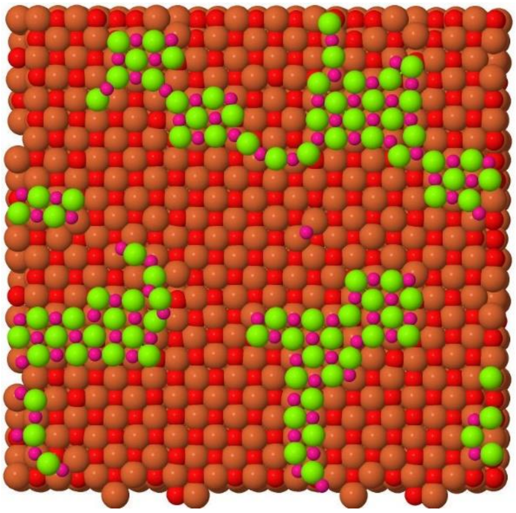

(b)

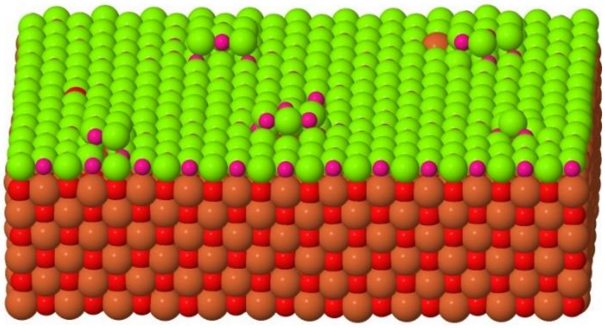

Figure 1. Snapshot of (a) 0.2 and (b) 1.1 MgO monolayers deposited on a MgO (001) substrate. The Mg^{2+} and O^{2-} ions of the substrate are colored light green and magenta respectively, whilst those of the thin film are brown and red.

(a)

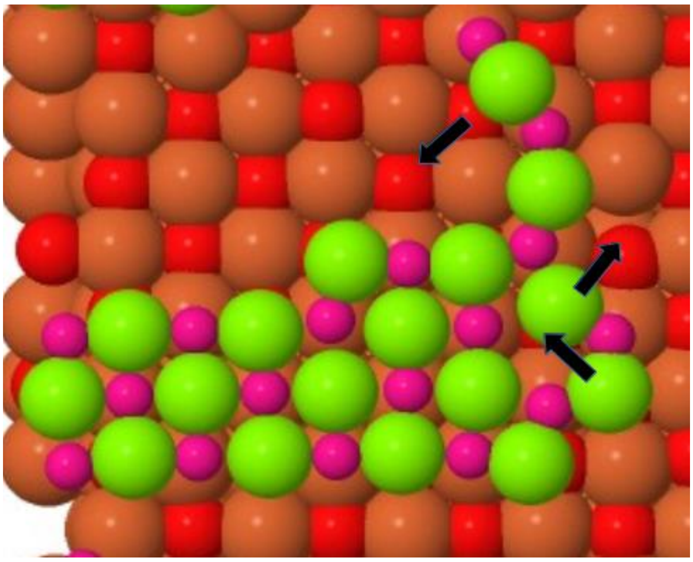

(b)

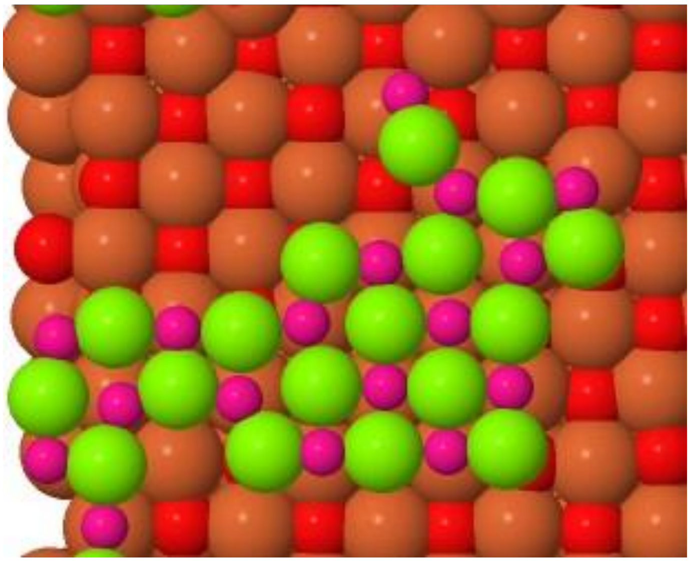

Figure 2. Atom positions before (a) and after (b) of a complex event that involves the translation of multiple atoms. The Mg^{2+} and O^{2-} ions in the substrate are brown and red respectively, whilst the green and magenta represent Mg^{2+} and O^{2-} ions in the thin film. The arrows indicate the direction of displacement.

(a)

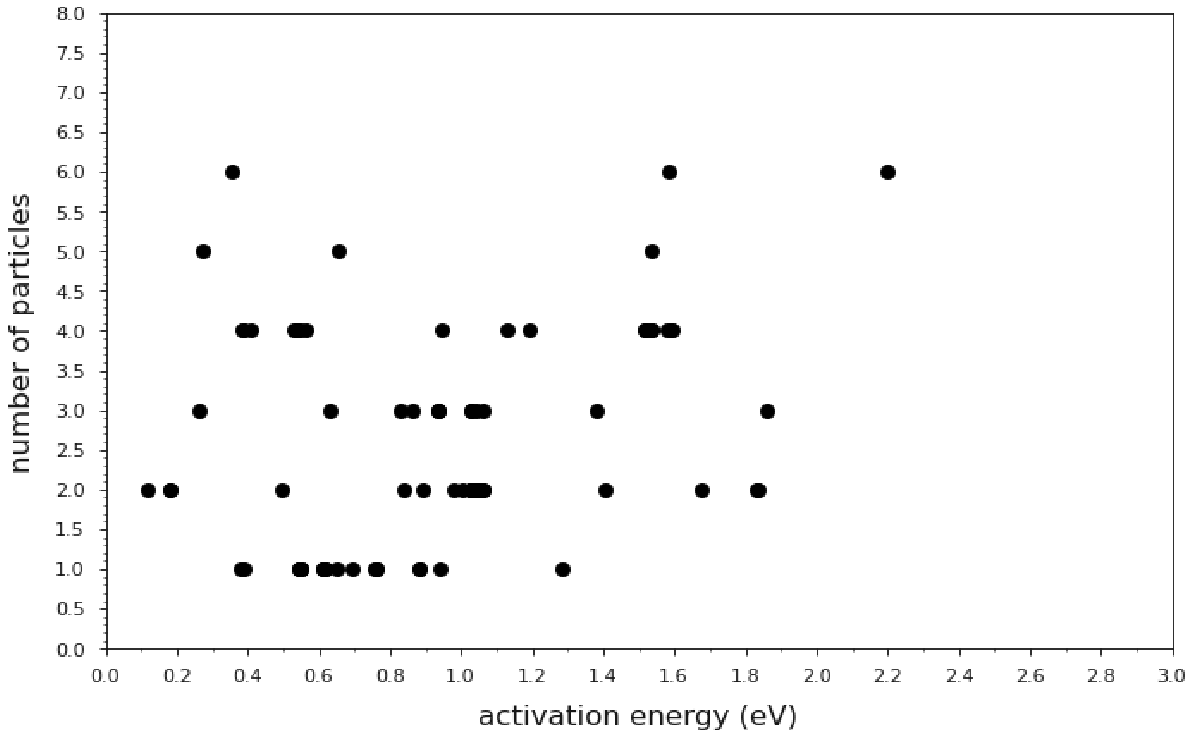

(b)

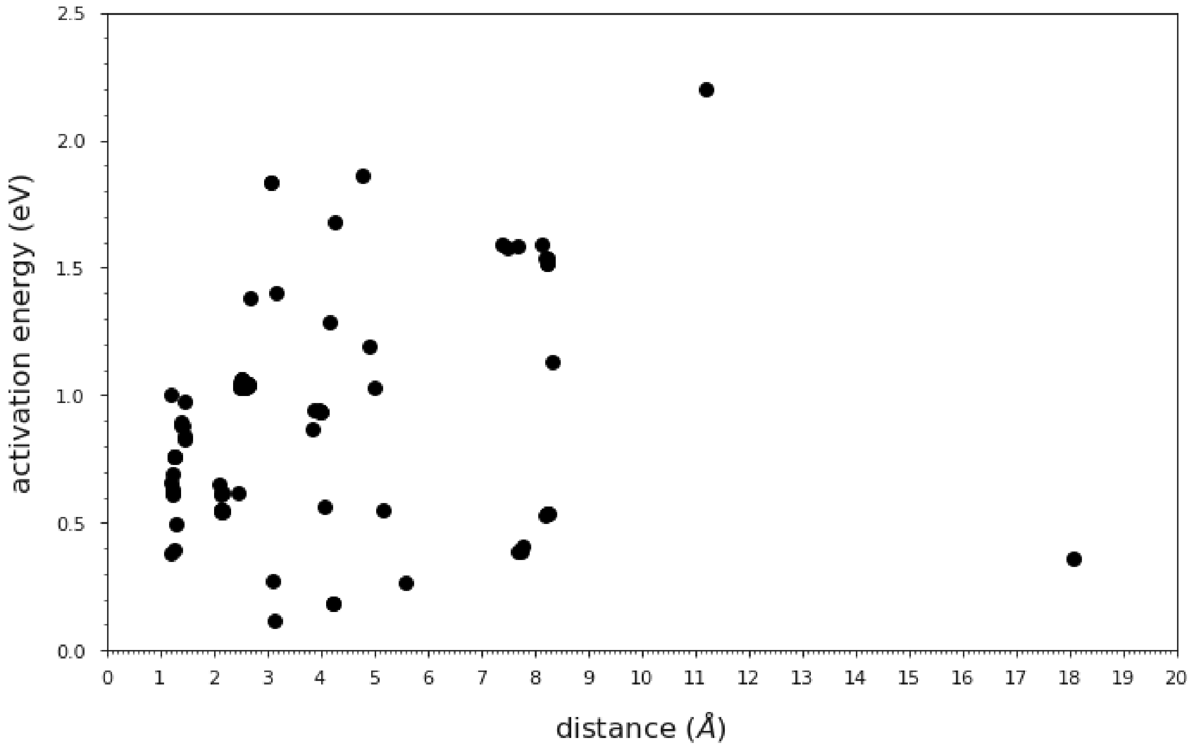

Figure 3. (a) The number of particles involved in a single diffusion event plotted against its calculated activation energy. (b) The activation energy vs the total distance of atoms moved. The data is obtained for 100 randomly chosen events when 120 Mg^{2+} and O^{2-} ions are allowed to diffuse on an MgO(001) surface.

MgO and CaO growth on a BaO(001) substrate.

It is not surprising that a layer-by-layer growth is observed for the MgO/MgO(001) interface and we now examine the growth of the binary oxides MgO and CaO on a BaO(001). In these simulations the bulk lattice parameter for the deposited materials (MgO and CaO) is less than that of the substrate. This in turn implies that the interactions within the deposited (MgO or CaO) thin film are stronger than those between the thin film and the BaO(001) substrate. In addition, there is a significant mismatch between the lattice parameters of the thin film and substrate. Bulk MgO, CaO and BaO have lattice parameters of 4.20, 4.80 and 5.54 Å respectively and a significant relaxation of the ions is expected, providing a much more stringent test of the computational method. Moreover, the construction of an on-lattice list based KMC is very difficult due to the misalignment of the different lattices. As the atoms start to be deposited, the Mg^{2+} ions tend to locate above the O^{2-} ions of the substrate whereas the deposited O^{2-} ions of the thin film prefer the bridging position between two Ba^{2+} ions (see Figure 4). The activation energies for isolated Mg^{2+} and Ca^{2+} ions to hop to the neighboring energy basin are 0.54 eV and 0.48 eV, respectively. Again, we find that the diffusion of ions on the surface includes correlated motion of cations and O^{2-} ions (Figure 5).

The position and peak shape in the radial distribution functions (RDF's) reflect the structure of the thin film and the nature of the interface. Figure 6 reports the calculated RDF's for Mg-O_{TF}, Mg-O_S and Mg-Ba as well as O_{TF}-O_{TF}, O_{TF}-O_S and O_{TF}-Ba "bonds". Throughout the paper, the subscripts "TF" and "S" refer to the thin film and deposition substrate, respectively. The Mg-O_{TF} and O_{TF}- O_{TF} bond lengths for 30 Mg^{2+} and O^{2-} pairs on BaO(001) are approximately 1.84 Å and 2.7 Å respectively. These bond-lengths are slightly shorter than those found in the bulk oxides and are due to the MgO film adjusting to the lattice mismatch. The Mg-O_S distance is approximately 2.0 Å as the Mg^{2+} ions are situated above the oxygen ions of the substrate (the peak is narrow as the bond lengths is similar in magnitude). However, the O_{TF}-O_S and O_{TF}-Ba bond lengths are similar (~3.0 Å) as the O_{TF} ions favor a bridging position between two or more Ba^{2+} ions. The positioning of the oxygen ions due to the mismatch in bulk lattice parameters and resulting strain allows unexpected structures to form where lines or loops of ions exist. A similar observation was made in reference 36 and these configurations exhibit a broadened profile for the O_{TF}–Ba RDF's. The strength of interactions within the thin MgO film are greater than those between the thin film and substrate. As a result, the MgO grows by the formation islands that are elongated along the [110] direction.

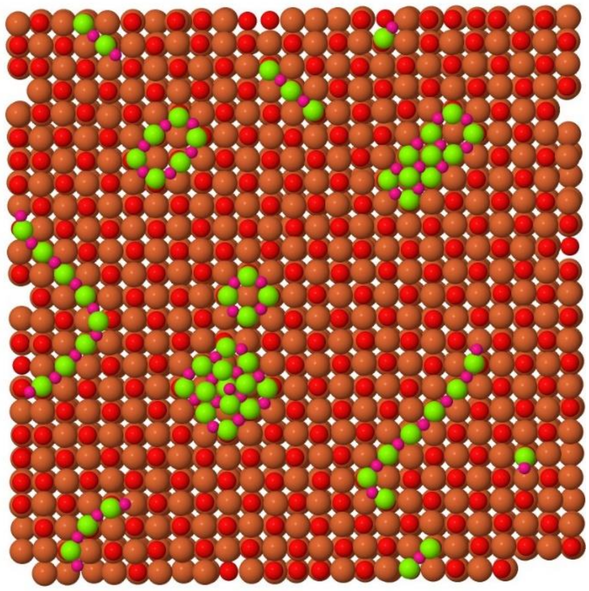

Figure 4. MgO (30 Mg^{2+} and 30 O^{2-} ions, 0.10 monolayers) that have been deposited on a BaO (001) substrate. Ba, O (substrate) are colored brown, red whilst the Mg and O ions (thin film) are green and magenta respectively.

(a)

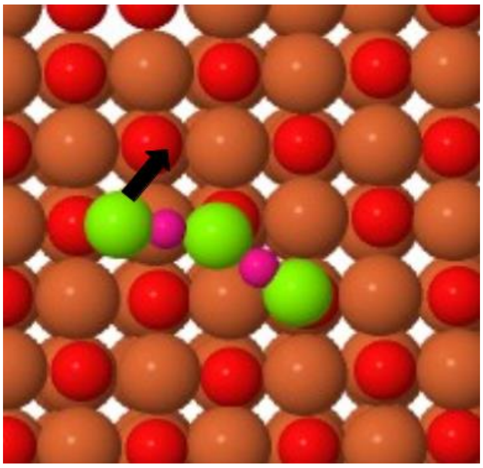

(b)

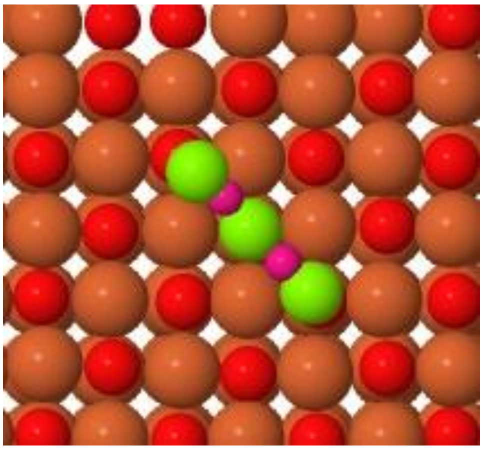

Figure 5. An example of correlated movement of an Mg^{2+} and O^{2-} ion (light green and magenta) on the BaO(100) surface (brown and red) to form a chain of ions. The activation energy for this event is 0.42 eV. The arrows indicate the direction of movement of the ions in the initial basin (a) to form the second basin (b).

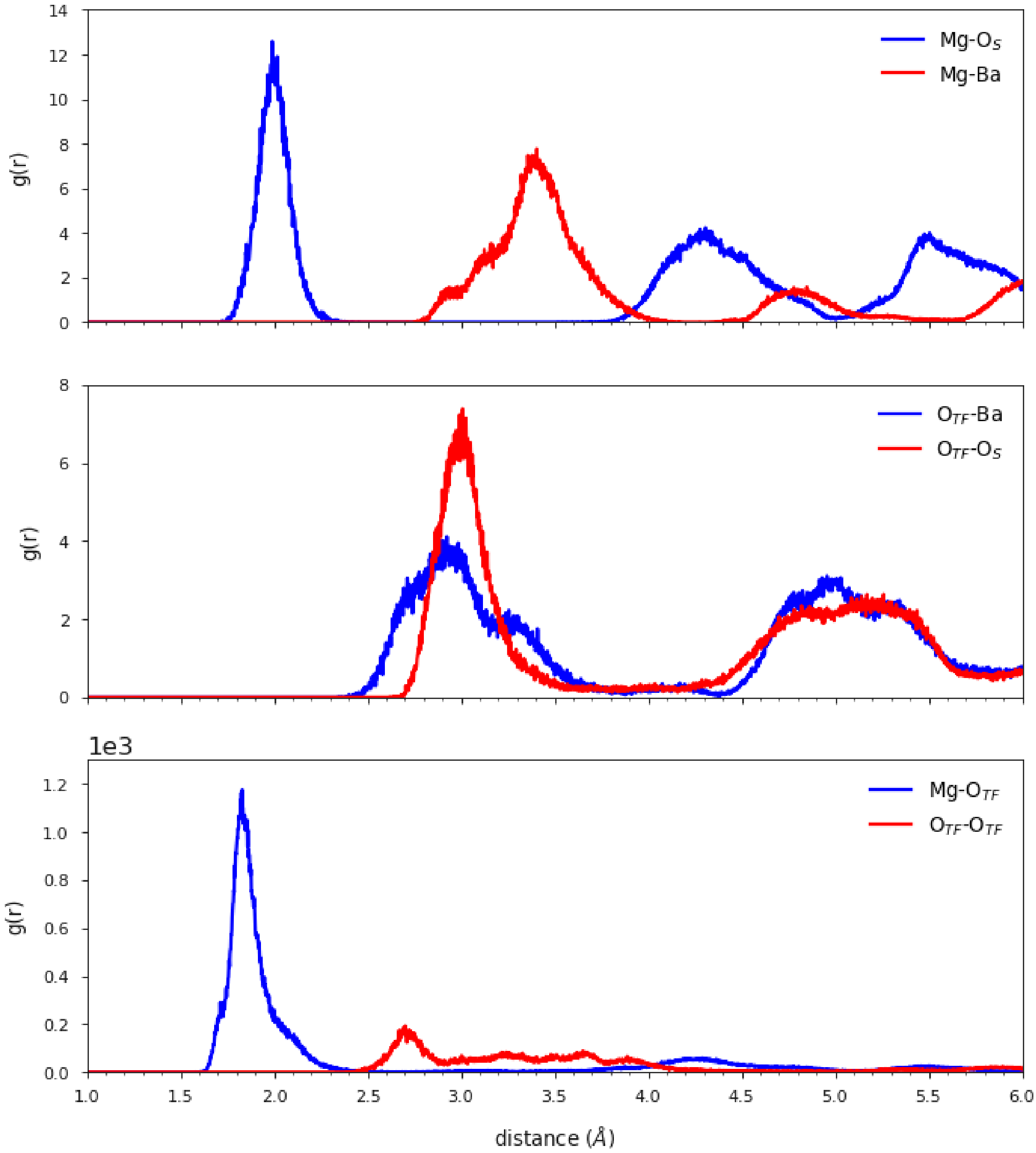

Figure 6. Calculated radial distribution functions (RDF's) for 30 Mg^{2+} and 30 O^{2-} ions on a Ba (001) substrate. The oxygen ions in the thin film and substrate are indicated by O_{TF} and O_S respectively. RDF's for the bulk oxides of MgO, CaO, SrO and BaO are presented in Figure S1 of the ESI for comparison with those of the thin film.

Figure S2 in the ESI displays several stages of growth for the MgO thin film at coverages of 0.8, 1.5 and 2.0 monolayers. For a monolayer coverage, isolated islands are still present as it is energetically more favorable for Mg^{2+} and O^{2-} ions to form additional layers (ESI figure S2b) rather than a single layer of evenly distributed ions (even for 0.8 monolayer coverage Mg^{2+} and O^{2-} ions can be observed to be situated on top of other Mg^{2+} and O^{2-} ions). After the deposition of two monolayers, the MgO ions have not formed a continuous thin film, but interconnected islands (ESI figure 2c) that persist even up to the deposition of the equivalent of 3 monolayers of ions (Figure 7). The calculated RDF's (Figure S3 in the ESI) obtained from the configuration in Figure 7 have well defined, narrow peaks for the intra thin film whilst the thin-film/substrate interactions are broad and less well defined. X-ray Reflectivity and Near-Edge X-ray Absorption Fine Structure measurements indicate that MgO grows to form well-structured thin films with coordination similar to MgO bulk.[37,38] We stress that while the computational demands of our calculations do not allow us to study thin films of comparable dimensions to those in reference 4, they do allow study of how the MgO/BaO(001) interface develops over a realistic (ms-long) time scale. The amorphization and recrystallization method identified the structure of the MgO/BaO(001) interface as comprising of misaligned MgO crystallites.[4] These crystallites included a central plateau area (MgO(100)/BaO(100)) containing dislocations and a vicinal MgO(111)/BaO(001) interface. We do not observe any dislocations, crystallites or MgO(111)/BaO(001) interfaces in our calculations as the longer timescales enable the system to suitably relax, *i.e.* the dislocations are likely an artefact of the amorphization and recrystallization approach.

We find that CaO growth on the BaO(001) substrate follows a similar mechanism, although the formation of islands is less marked since the difference in lattice parameters of the binary oxides is less than that at the MgO/BaO interface and the strength of the Ca-O_{TF} interaction is less than that for Mg-O_{TF}. Figure 8 and Figure S4 in the ESI display snapshots of the structure observed for 0.8 and 2 monolayers of Ca^{2+} and O^{2-} ions on the BaO(001) surface, respectively. Mohn *et al.* also studied the CaO/BaO(001) interface using manual creation of islands and clusters followed by energy minimization. The authors observed the formation of a domain structure in their study of CaO/BaO(001) interfaces.[10] In contrast, we observe the formation of three-dimensional islands rather than two-dimensional domains, despite using the same interatomic potentials. We speculate that this is due to the strongly biased sampling of configurational space by the manual approach in Ref. 10, which intrinsically prevents exploration of the thermal dynamics and mechanisms of island growth. The Ca-O_S and O_{TF}-

Ba RDF's (Figure 9) have similar distances to those in the bulk materials whilst those for the interactions between the thin film and substrate do not demonstrate the same degree of distortion as for the MgO/BaO(001) interface.

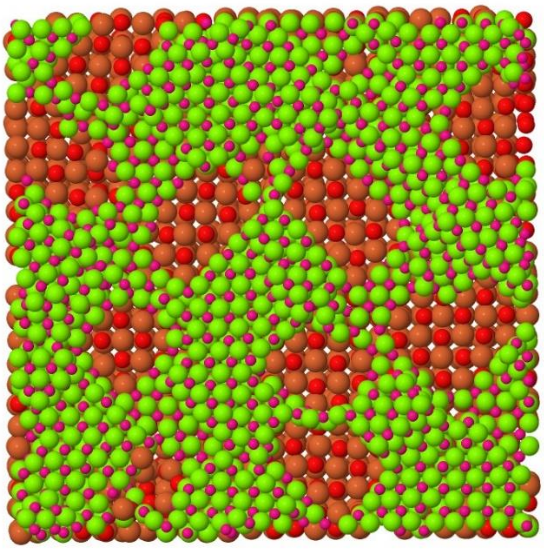

Figure 7. The equivalent of 3 monolayers of MgO on BaO(001). Ba, O (substrate) are colored brown, red whilst the Mg^{2+} and O^{2-} ions (thin film) are light green and magenta respectively.

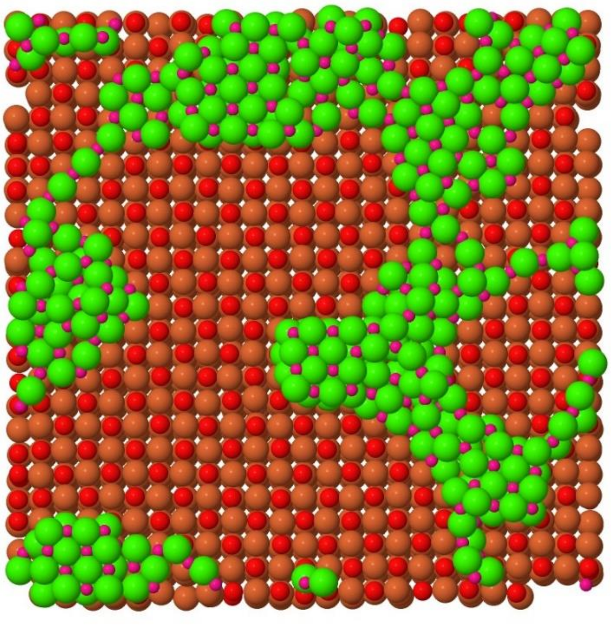

Figure 8. 0.8 monolayers of CaO deposited on a BaO (001) substrate. Ba, O (substrate) are colored brown, red and Ca and O (thin film) are light green and magenta respectively.

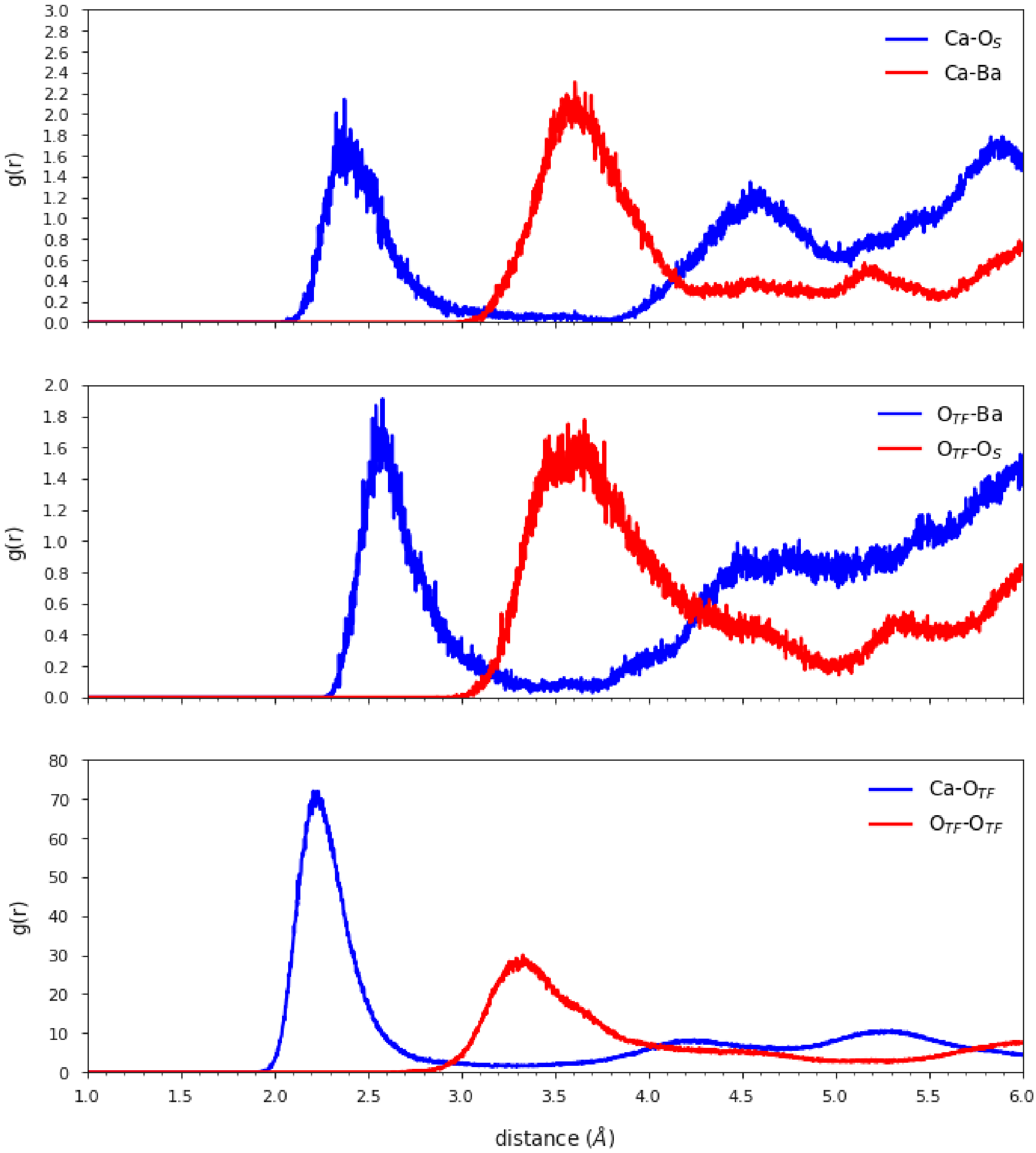

Figure 9. RDF's for 2 monolayers of CaO grown on a BaO (001) surface.

CaO and SrO growth on a MgO(001) substrate.

In these examples, the bulk lattice parameter for the components of the thin film is greater than that of the substrate. First, we examine the CaO thin film on MgO. The Ca^{2+} ions prefer to sit above the O^{2-} ions of substrate and the O_{TF} above the Mg^{2+} ions of the substrate (Figure S5 in the ESI). Deposition of a monolayer of CaO (Figure S5b) growth gives rise to the formation of a CaO over layer. However, the mismatch in spacing results in defects in the form of both cation and anion "vacancies". The ions that cannot be accommodated in the monolayer form islands that are often 2 particles in depth (Figure S5b). Further deposition and growth of the thin film result in the formation of continuous, but distorted, layers. For example, 2 monolayers creates a thin film that is approximately 3 layers in depth, but is distorted so that steps in the surface are formed (Figure 10a). Where 3 monolayers of CaO have been deposited (Figure 10b) the strain in the CaO/MgO interfacial layers is relaxed by lattice distortion and misfit dislocations that grow almost perpendicular to the surface. The Ca-O_{TF}, Ca-O_S and O_{TF}-O_S RDF's have well defined peaks indicating a well-structured over layer (Figure S6 in the ESI). The lattice parameter of SrO is greater still and the formation of an coincident/ideal monolayer would result in significant compression of the Sr-O and O-O "bonds". This level of compression is energetically not feasible and results in buckling of the thin film at the interface and the RDF's of Sr-O_S and O_{TF}-O_S are broad and no longer exhibit well defined peaks (Figure S7 in the ESI). The structure of CaO and SrO films on MgO(001) have been examined in reference 39 using X-ray diffraction and transmission electron microscopy and CaO films on MgO(001) by high-resolution transmission electron microscopy (HRTEM) in reference.[40] Both CaO(001) and SrO(001) films are observed to grow on the surface of MgO. In addition, our calculations exhibit excellent agreement the structure of misfit dislocations and distortions of the lattice to accommodate the misfit strain identified in the HRTEM experiments. In addition, calculations employing energy minimization identified hexagonal BaO structures that were "buckled" with limited contact with the MgO crystal surface (Figure 10).[36]

(a)

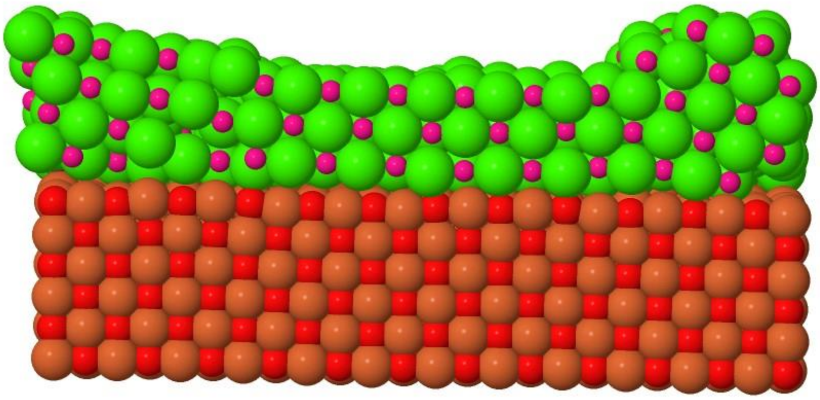

(b)

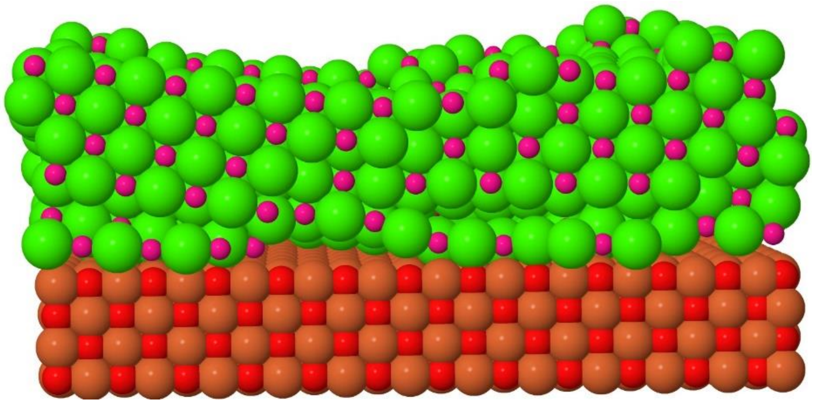

Figure 10. (a) Two and (b) Three monolayers of CaO deposited on a MgO (001) substrate. Mg, O (substrate) are colored brown, red and Ca and O (thin film) are light green and magenta respectively.

Conclusions

We have constructed a multiscale workflow, combining Monte Carlo/MD and adaptive kinetic Monte Carlo simulations to study the growth of oxide thin films in contrast to prior calculations. MD is used to simulate the deposition of ions on the surface whilst KMC is employed to study diffusion of ions at the surface and the re-organization of the ions at the interface over a total time of approximately 0.5 milli-seconds (i.e. times that are not easily accessible to MD at room temperature). We have demonstrated the limitations of previous calculations. The amorphisation and recrystallization method generates thin films that contain a large number of dislocations/grain boundaries. We hypothesize that this results from the configuration “freezing” at an (arbitrary) high temperature and that the thin film fails to reach a minimum energy configuration. The alternate approach of manually sampling configurations is impractical and inadequate for sufficient sampling phase space. Therefore, we emphasize that the kinetic Monte Carlo component of the simulation strategy is required to allow the diffusion of cations and anions so that they can organize into a structured thin film.

To evaluate the suitability of the workflow we have examined the growth of binary oxides on a range substrates. When considering MgO growth on MgO the adsorbate-surface and adsorbate-adsorbate interactions are identical and a "layer-by-layer" (Frank-van-der-Merwe) growth is observed. In contrast, for MgO and CaO growth on BaO the thin film-surface interactions are weaker than those for the absorbate-absorbate and we observe the growth of isolated islands. We do not observe the crystallites and dislocations that were found with the amorphization and recrystallization method. We attribute the origin of this difference to the much longer time scales employed in our simulations, which warrant for unbiased relaxation of the deposited atoms. In addition, sampling configuration space manually is difficult and likely to lead to incorrect conclusions on thin film growth. We have also modeled CaO and SrO growth on MgO (001) where the lattice parameter is greater than the substrate. For CaO, the adsorbate-surface interactions are stronger than adsorbate-adsorbate interactions and we observe a layer-plus-island growth mechanism (Stranski-Krastanov). We find that a distorted structure is created when SrO thin films are grown on MgO (001).

Our pilot study has demonstrated that a computational approach to understanding the design of ultrathin films is feasible and could be combined with suitable experiments as well as more accurate force and energy evaluation methods (e.g. by linear-scaling Density Functional Theory[41]) to examine the growth conditions for specific and technologically important applications.

Supplementary Material

The supplementary material contains additional figures referenced in the text.

Acknowledgments

Computing resources provided by STFC Scientific Computing Department's SCARF cluster. This work is supported by the Ada Lovelace Centre - a joint initiative between the Science and Technology Facilities Council (as part of UK Research and Innovation), Diamond Light Source and the UK Atomic Energy Authority. The authors would like to thank Drs Paul Donaldson and Stephen Hull for useful discussions.

Data Availability

The data that support the findings of this study are available from the corresponding author upon reasonable request.

References

---

[1] H. Y. Hwang, Y. Iwasa, M. Kawasaki, B. Kelmer, N. Nagaosa, and Y. Tokura, Nature Materials 11, 103 (2012).

[2] J. Chakhalian, A.J. Millis; and J. Rondinelli, Nature Materials 11, 92 (2012).

[3] X. Yang, Z. Zhou, T. Nan, Y. Gao, G. M. Yang, M. Liu, and N. X. Sun, J. Mat. Chem. C 4, 234 (2016).

[4] D. C. Sayle, and G. W. Watson, J. Mater. Chem.10, 2241(2000).

[5] D. C. Sayle, S. A. Maicaneanu, and G. W. Watson, Phys. Chem. Chem. Phys. 4, 5189 (2002).

[6] D. C. Sayle, and G. W. Watson, J. Phys. Chem. B 106, 3916 (2002).

[7] L. Vernon, S. D. Kenny, R. Smith, and E. Sanville, Phys. Rev. B 83, 075412 (2011).

[8] M. Yu, and S. D. Kenney, J. Phys.: Condens. Matter. 28, 105002 (2016).

[9] G. Henkelman and H. Jónsson, J. Chem. Phys. 115, 9657 (2001).

[10] C. E. Mohn, N. L. Allan, and J. H. Harding, Chem. Phys. Phys. Chem. 11, 3217 (2009).

[11] C. E. Mohn, M. J. Stein, and N. L. Allan, J. Mater. Chem. 20, 10403 (2010).

[12] L. Xu, and G. Henkelman, J. Chem. Phys. 129, 114104 (2008).

[13] P. Tiwary, and A. van de Walle, Phys. Rev. B 87, 094304 (2013).

[14] Y-Q Su, J.-X. Liu, I. A. W. Filot, and E. J. M. Hensen, Chem. Mater. 29, 9456 (2017).

[15] A. L. Lloyd, Y. Zhou, M. Yu, C. Scott, R. Smith, and S. D. Kenny, J. Chem. Phys. 147, 152719 (2017).

[16] A. V. Brukhno, J. Grant, T. L. Underwood, K. Stratford, S. C. Parker, J. A. Purton, and N. B. Wilding, Molecular Simulation 47, 131 (2021).

[17] W. Smith, and T. Forester, J. Mol. Graphics 14, 136 (1996).

[18] D. T. Gillespie, J. Phys. Chem. 81, 2340 (1977).

[19] A. F. Voter, Phys. Rev. B 34, 6819 (1986).

[20] C. Battaile, Comput. Methods Appl. Mech. Engrg. 197, 3386 (2008).

[21] P. P.Dholabhai, S. Anwar, J. B. Adams, P. Crozier, and R. Sharma, J. Solid State Chem. 184, 811 (2011).

[22] D. Frenkel and B. Smit, *Understanding Molecular Simulation: From Algorithms to Applications*, Academic Press (2002).

---

[23] G. Henkelman, and H. Jónsson, J. Chem. Phys. 111, 7010 (1999).

[24] G. T. Barkema, and N. Mousseau, Computational Materials Science 20, 285 (2001).

[25] E. Bitzek, P. Koskinen, F. Gähler, M. Moseler, and P. Gumbsch, Phys. Rev. Lett. 97, 170201 (2006).

[26] M.R. Sørensen, K.W. Jacobsen, and H. Jónsson, Phys. Rev. Lett 77, 5067 (1996).

[27] G. Henkelman and H. Jónsson, J. Chem. Phys. 113, 9978 (2000).

[28] D. Hamelberg, J. Mongan, and J. A McCammon, J. Chem. Phys. 120, 11919 (2004).

[29] G. V. Lewis, and C.R.A. Catlow, J. Phys. C 18, 1149 (1985).

[30] P. P. Ewald, Ann. Phys. (Leipzig) 64, 253 (1921).

[31] G. Henkleman, B. P. Uberuaga, D. J. Harris, J. H. Harding, and N. L. Allan, Phys. Rev. B 72, 115437 (2005).

[32] G. Geneste, J. Morillo and F. Finocchi, J. Chem. Phys., 122, 174707 (2005).

[33] D. J. Harris, M. Yu Lavrentiev, J. H. Harding, N. L. Allan, and J. A. Purton, J. Phys. Condens. Matter. 16, L187 (2004).

[34] E. Antoshchenkova, M. Hayoun, F. Finochi, and G. Geneste, Surface Science 606, 605 (2012).

[35] S. A. Chambers, T. T. Tran, and T. A. Tileman, J. Mat. Res. 9, 2944 (1994).

[36] D. C. Sayle, S. C Parker, and J. H. Harding, J. Mater. Chem. 4, 1883 (1994).

[37] J. P. Singh, W. C. Lim, Ik-J. Lee, S. O. Won,; K. H. Chae, Science of Advanced Materials, 10, 1372 (2018).

[38] J. P. Singh and L. K. Gupta, International Journal of Mathematical, Engineering and Management Sciences 4, 619 (2019).

[39] P. A. Langjahra, T. Wagner, F. F. Lange and M. Rühlea, J. Cryst. Growth, 256, 162 (2003)

[40] H. D. Li, X. N. Zhang and Z. Zhang, Z. X. Mei, X. L. Du, and Q. K. Xue, J. Appl. Phys., 102, 046103 (2007).

[41] J. C. A. Prentice, J. Aarons, J. C. Womack, A. E. A. Allen, L. Andrinopoulos, L. Anton, R. A. Bell, A. Bhandari, G. A. Bramley, R. J. Charlton, R. J. Clements, D. J. Cole, G. Constantinescu, F. Corsetti, S. M.-M. Dubois, K. K. B. Duff, J. M. Escartín, A. Greco, Q. Hill, L. P. Lee, E. Linscott, D. D. O'Regan, M. J. S. Phipps, L. E. Ratcliff, Á. R. Serrano, E. W. Tait, G. Teobaldi, V. Vitale, N. Yeung, T. J. Zuehlsdorff, J. Dziedzic, P. D. Haynes, N. D. M. Hine, A. A. Mostofi, M. C. Payne, and C.-K. Skylaris, J. Chem. Phys. 152, 174111 (2020).

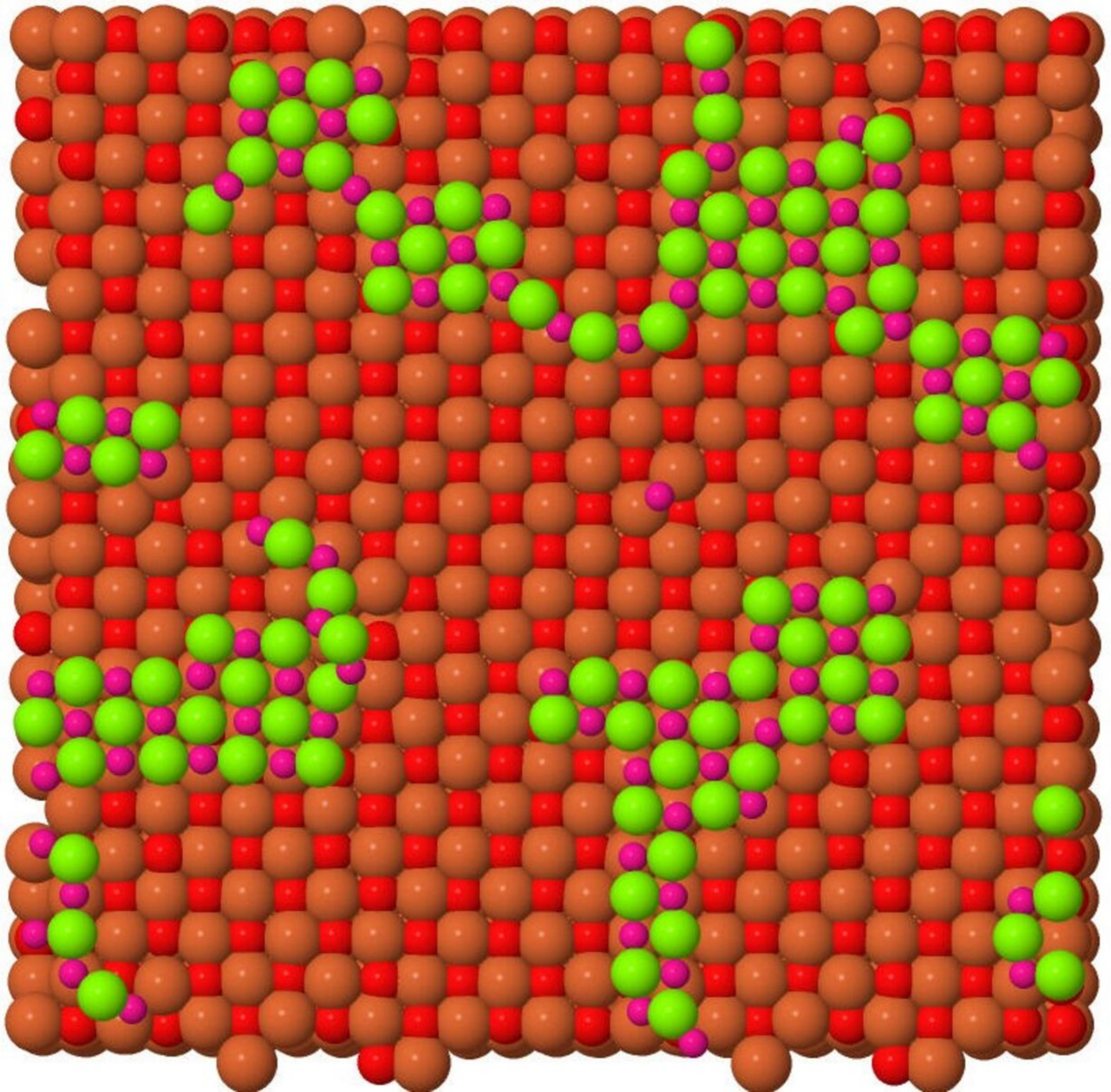

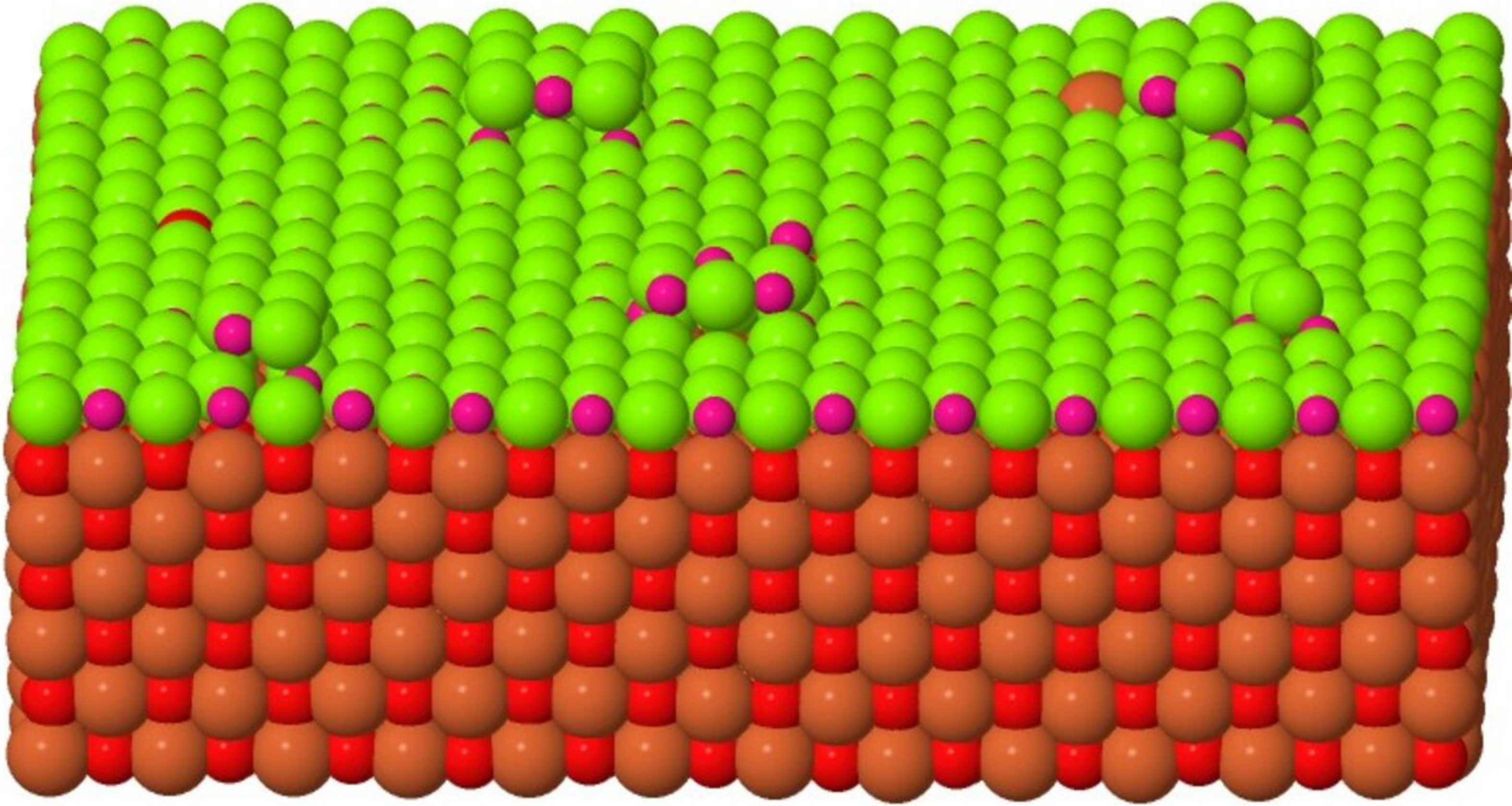

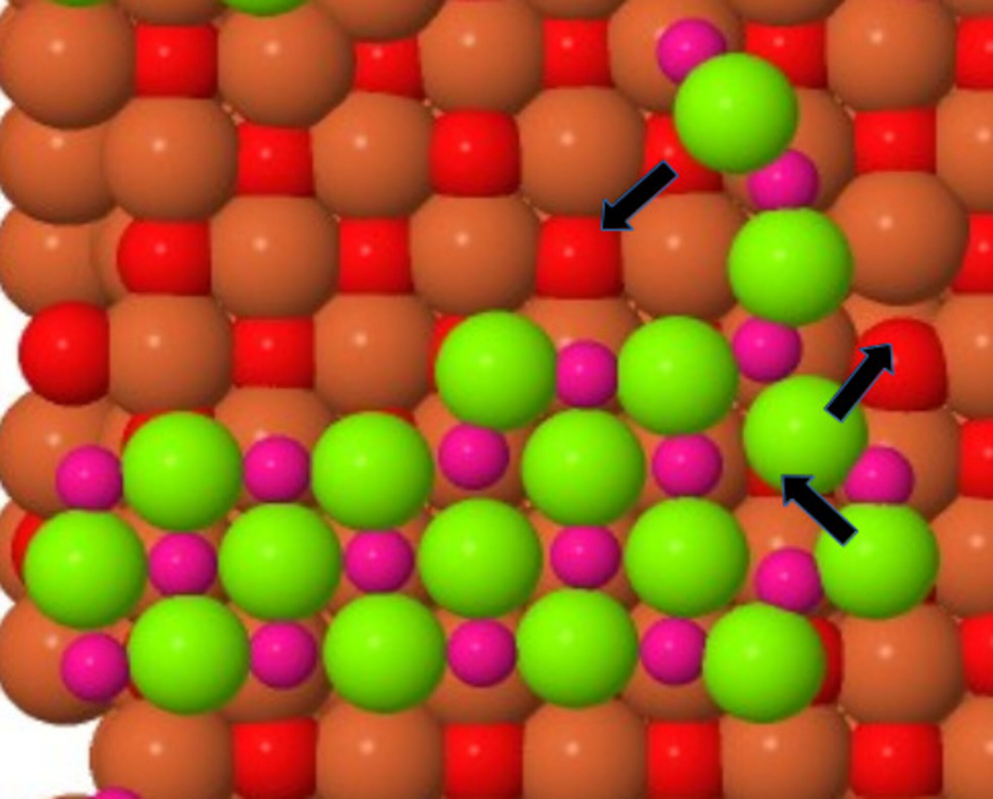

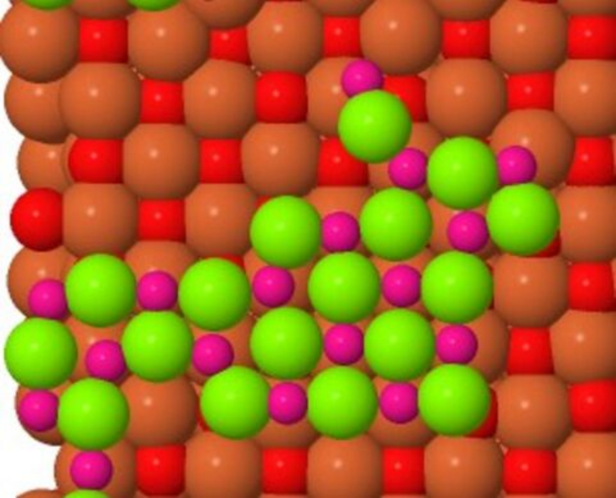

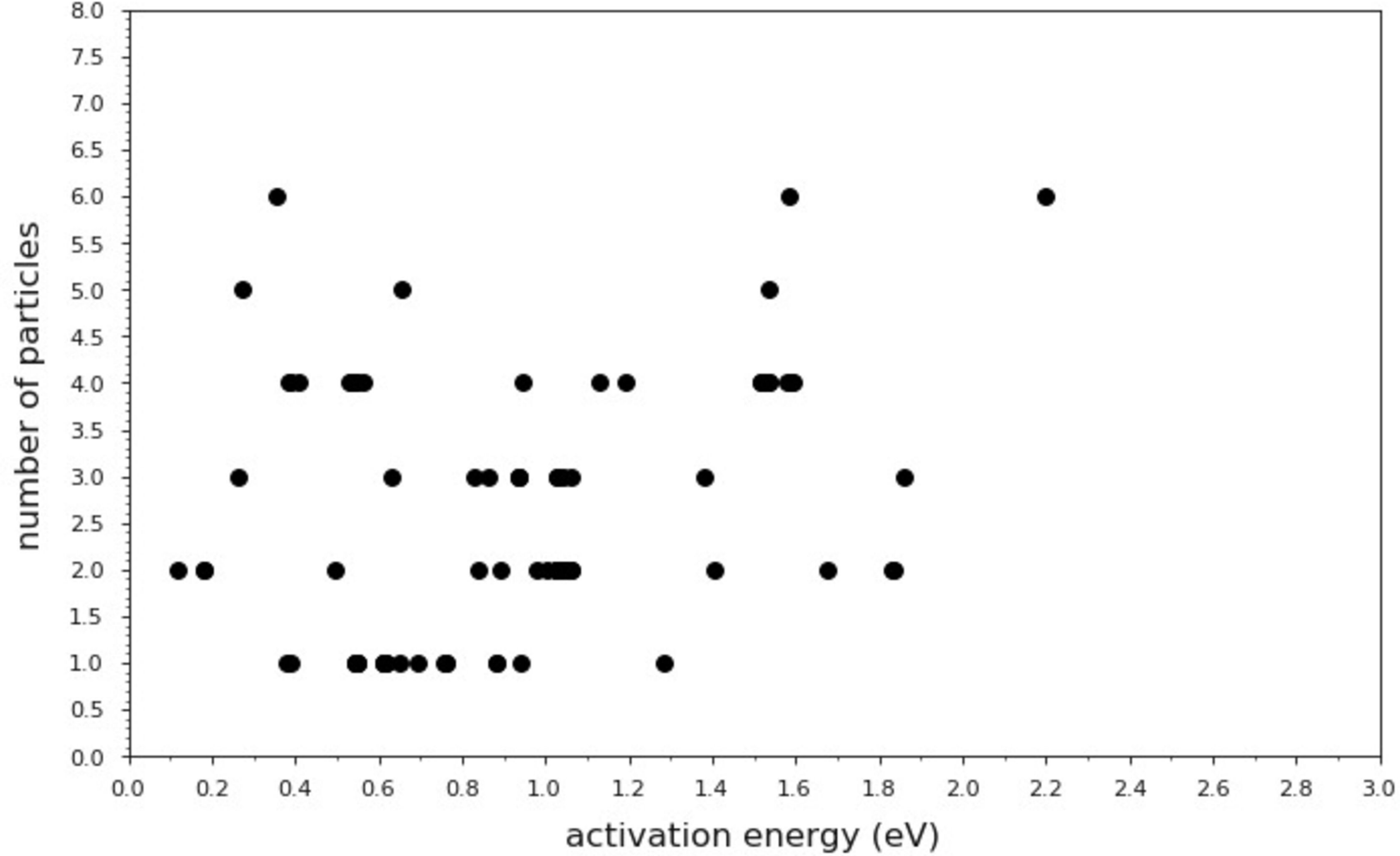
number of particles
8.0
7.5
7.0
6.5
6.0
5.5
5.0
4.5
4.0
3.5
3.0
2.5
2.0
1.5
1.0
0.5
0.0
0.0
0.2
0.4
0.6
0.8
1.0
1.2
1.4
1.6
1.8
2.0
2.2
2.4
2.6
2.8
3.0
activation energy (eV)

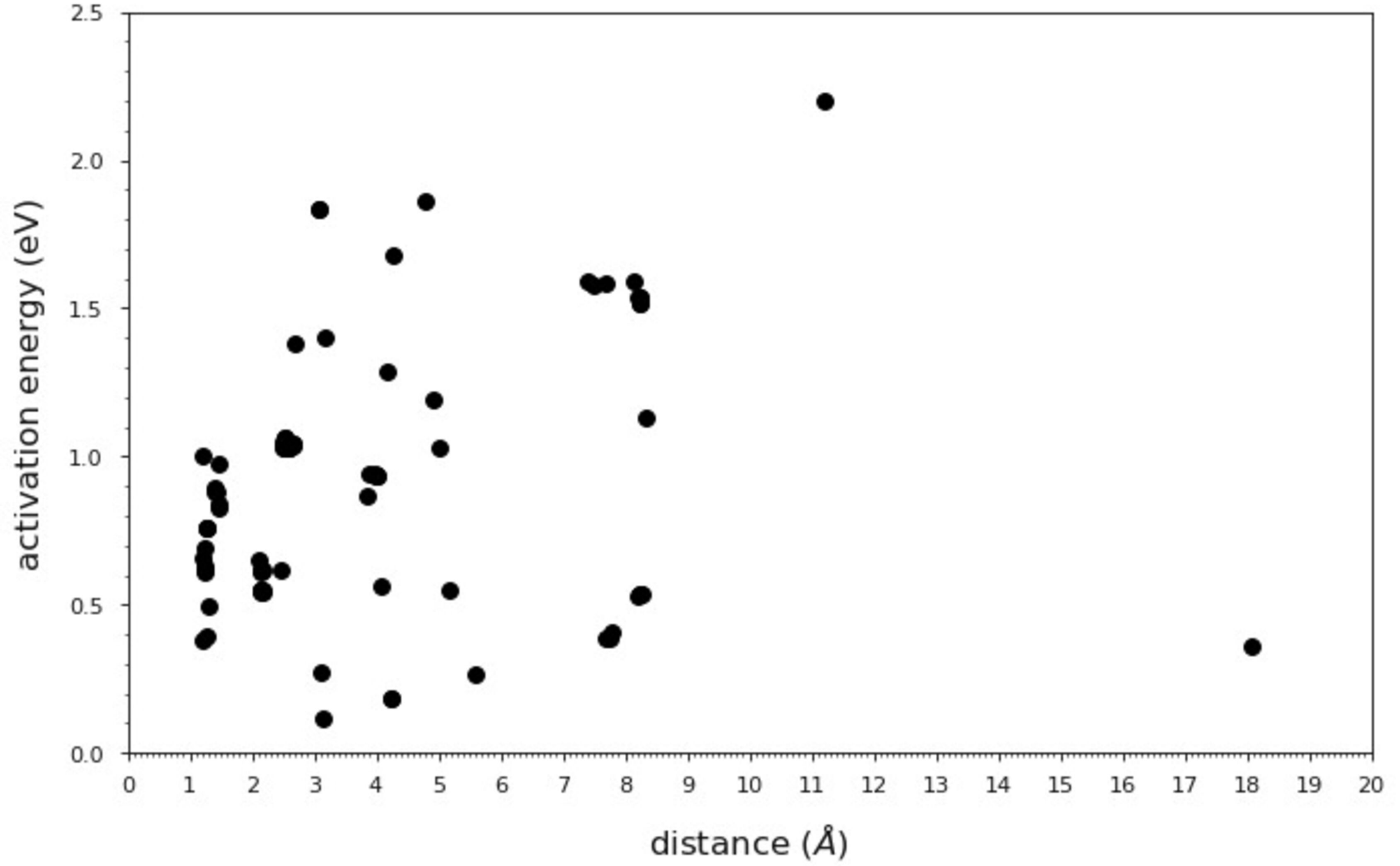
activation energy (eV)
2.5
2.0
1.5
1.0
0.5
0.0
0
1
2
3
4
5
6
7
8
9
10
11
12
13
14
15
16
17
18
19
20
distance (Å)

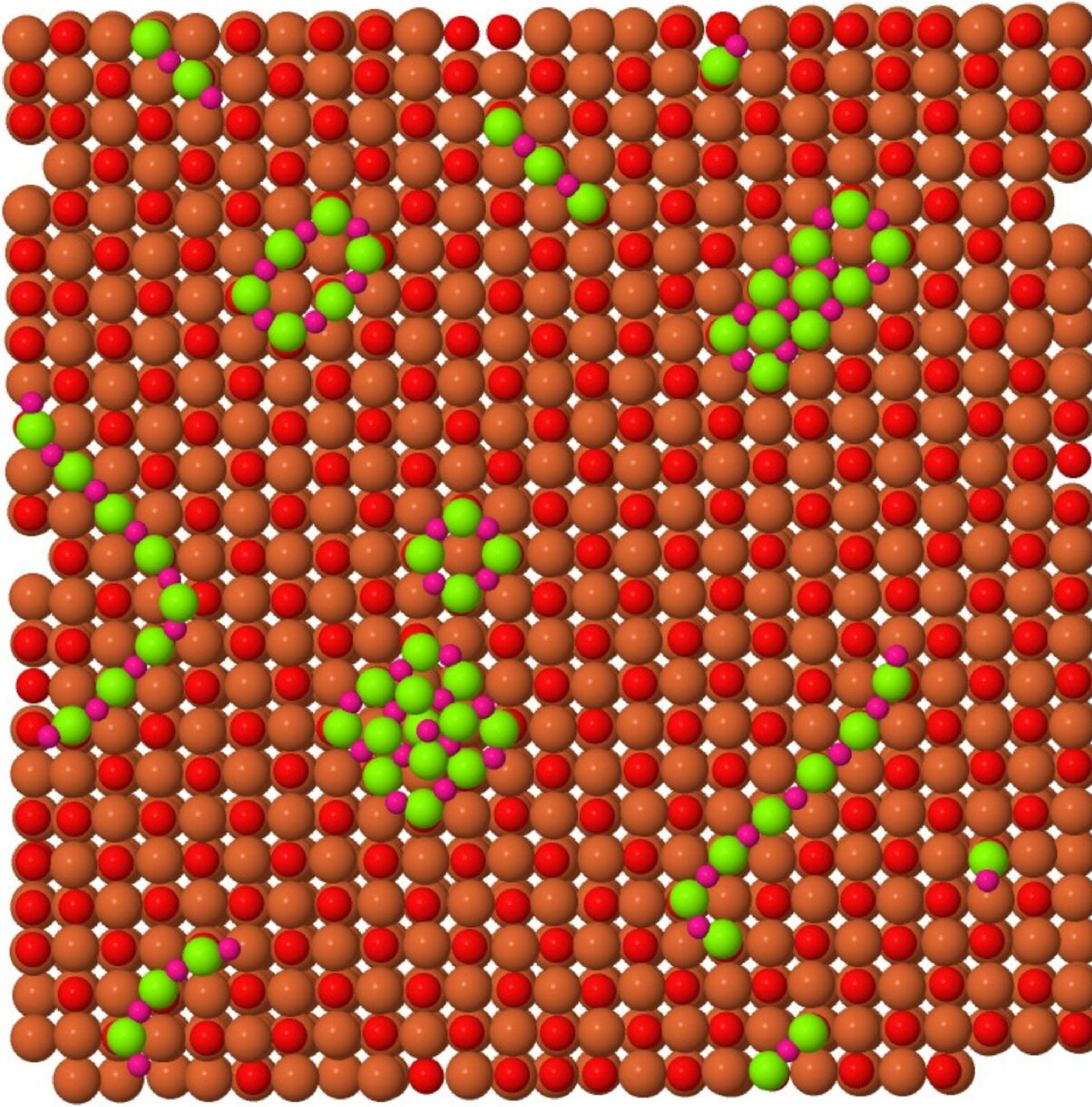

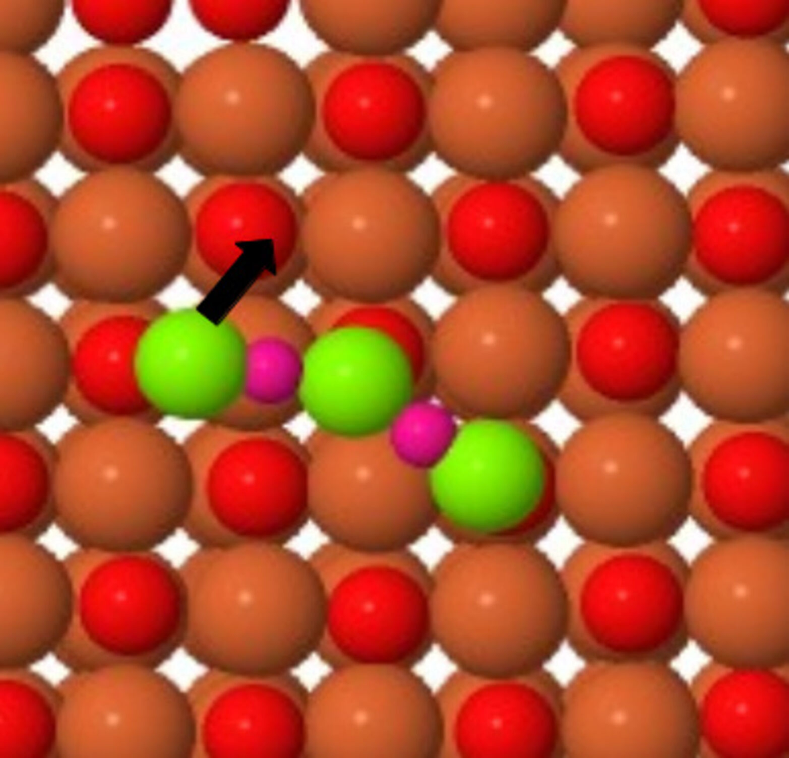

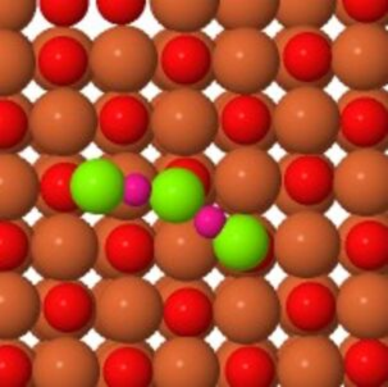

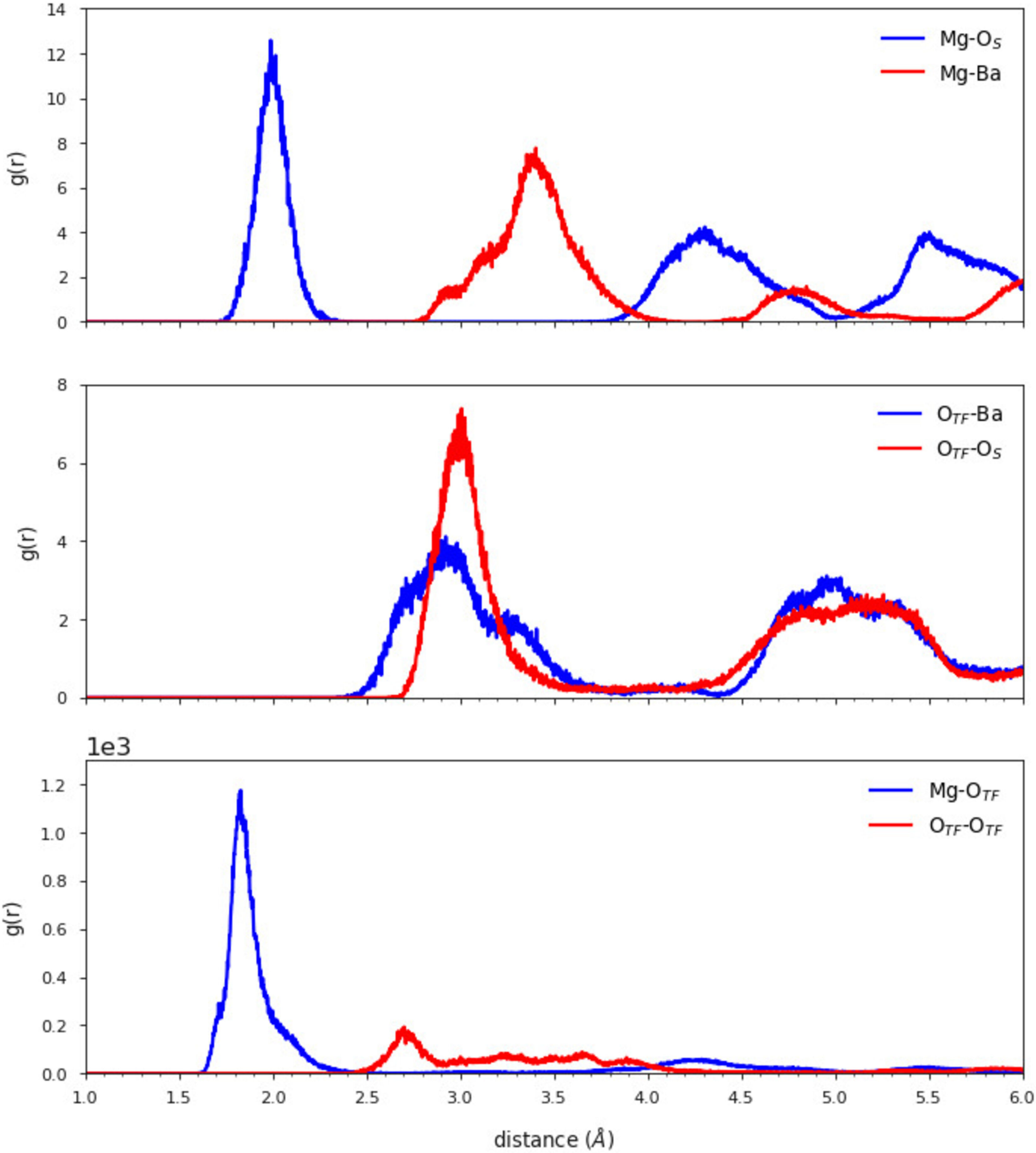
Mg-O$_S$
Mg-Ba
O$_{TF}$-Ba
O$_{TF}$-O$_S$
Mg-O$_{TF}$
O$_{TF}$-O$_{TF}$
g(r)
0
2
4
6
8
10
12
14
g(r)
0
2
4
6
8
1e3
g(r)
0.0
0.2
0.4
0.6
0.8
1.0
1.2
1.0
1.5
2.0
2.5
3.0
3.5
4.0
4.5
5.0
5.5
6.0
distance (Å)

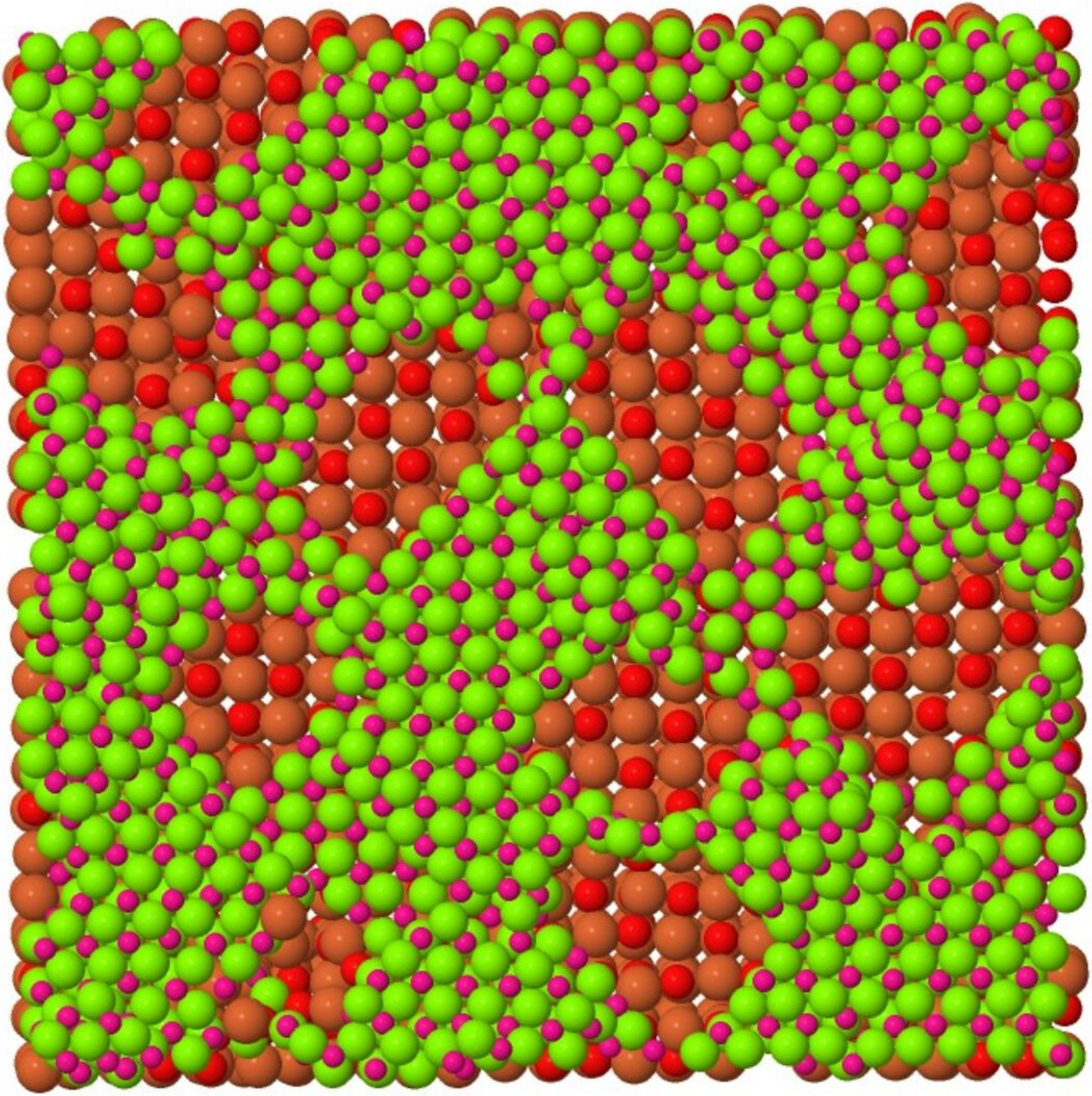

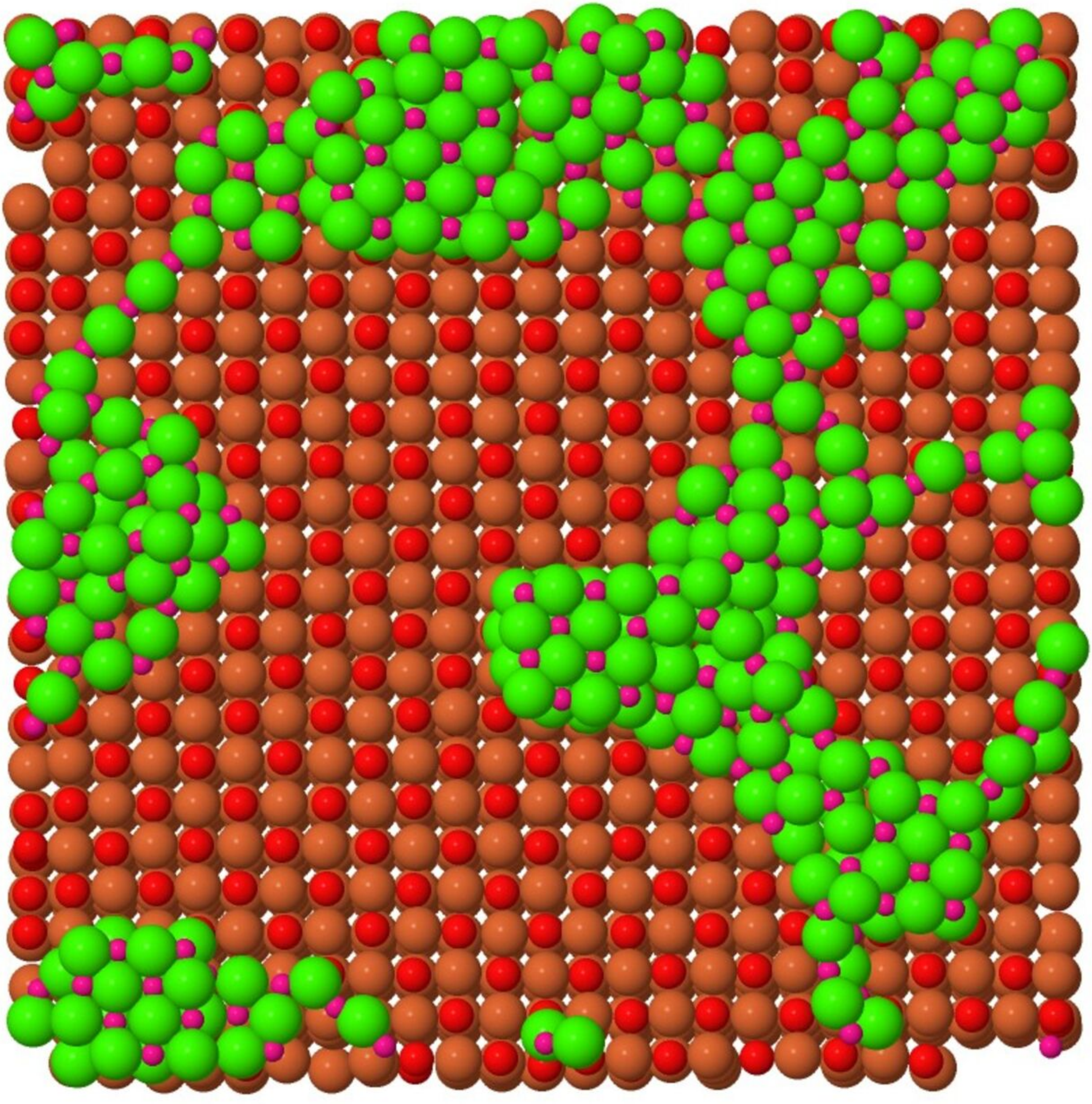

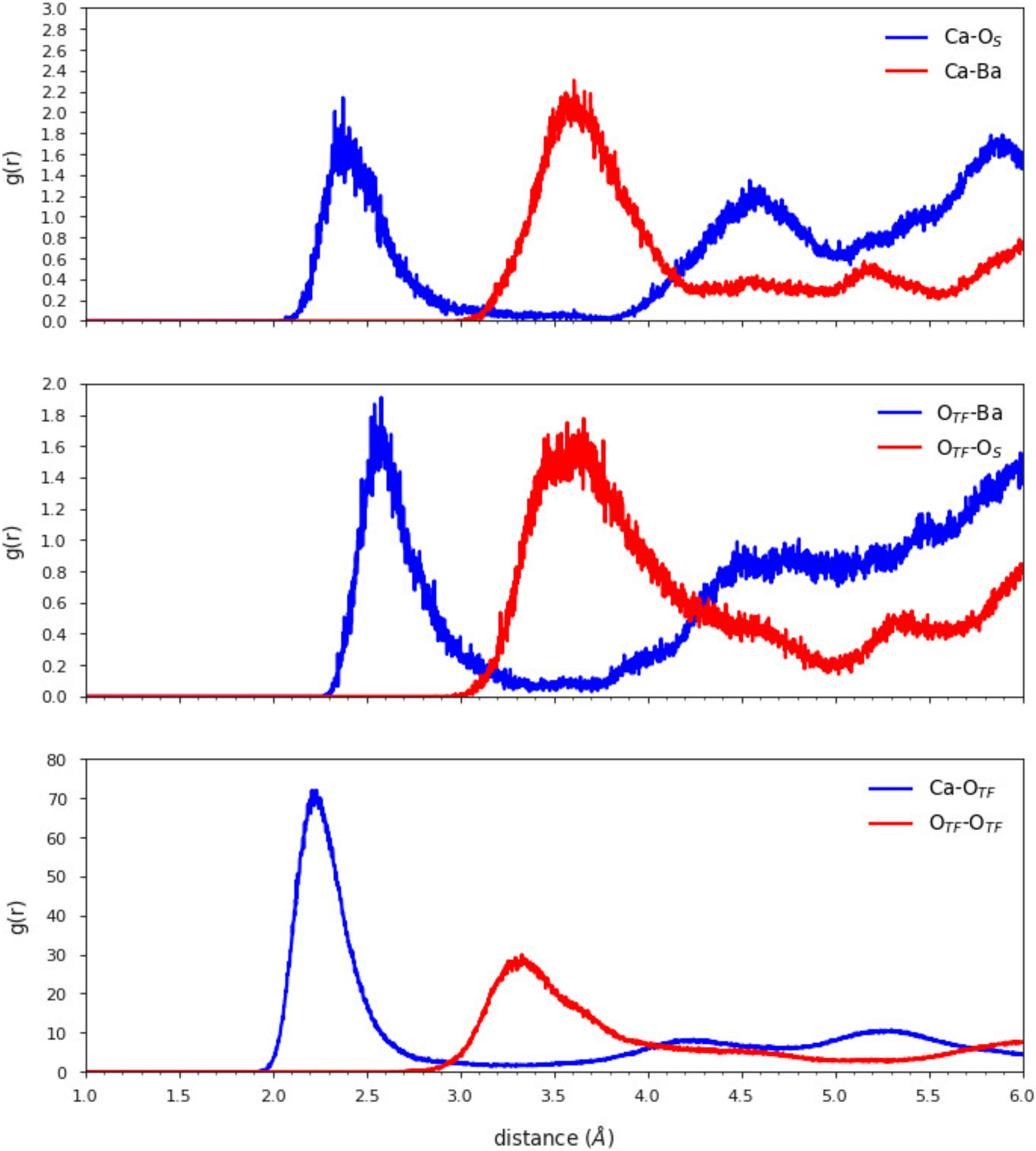

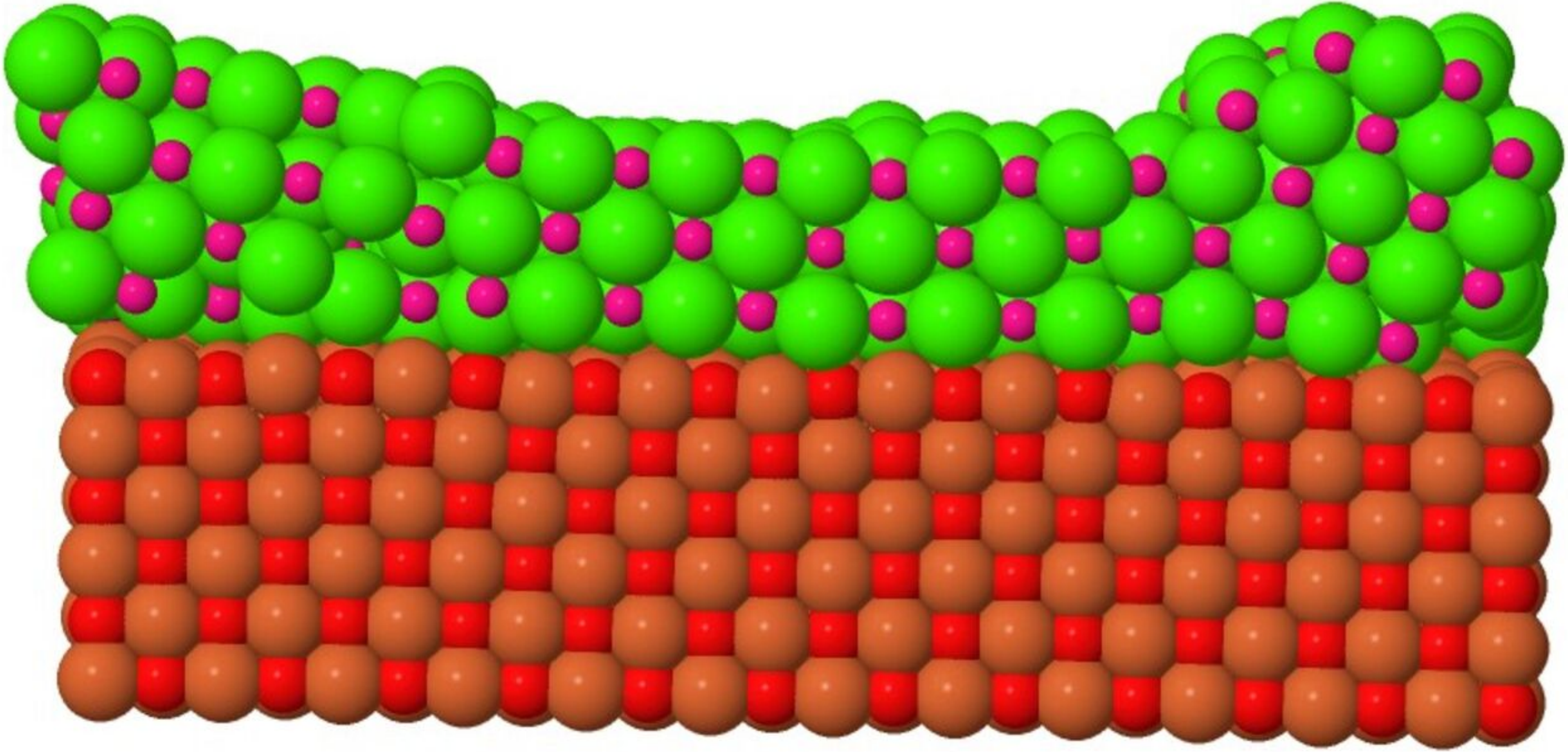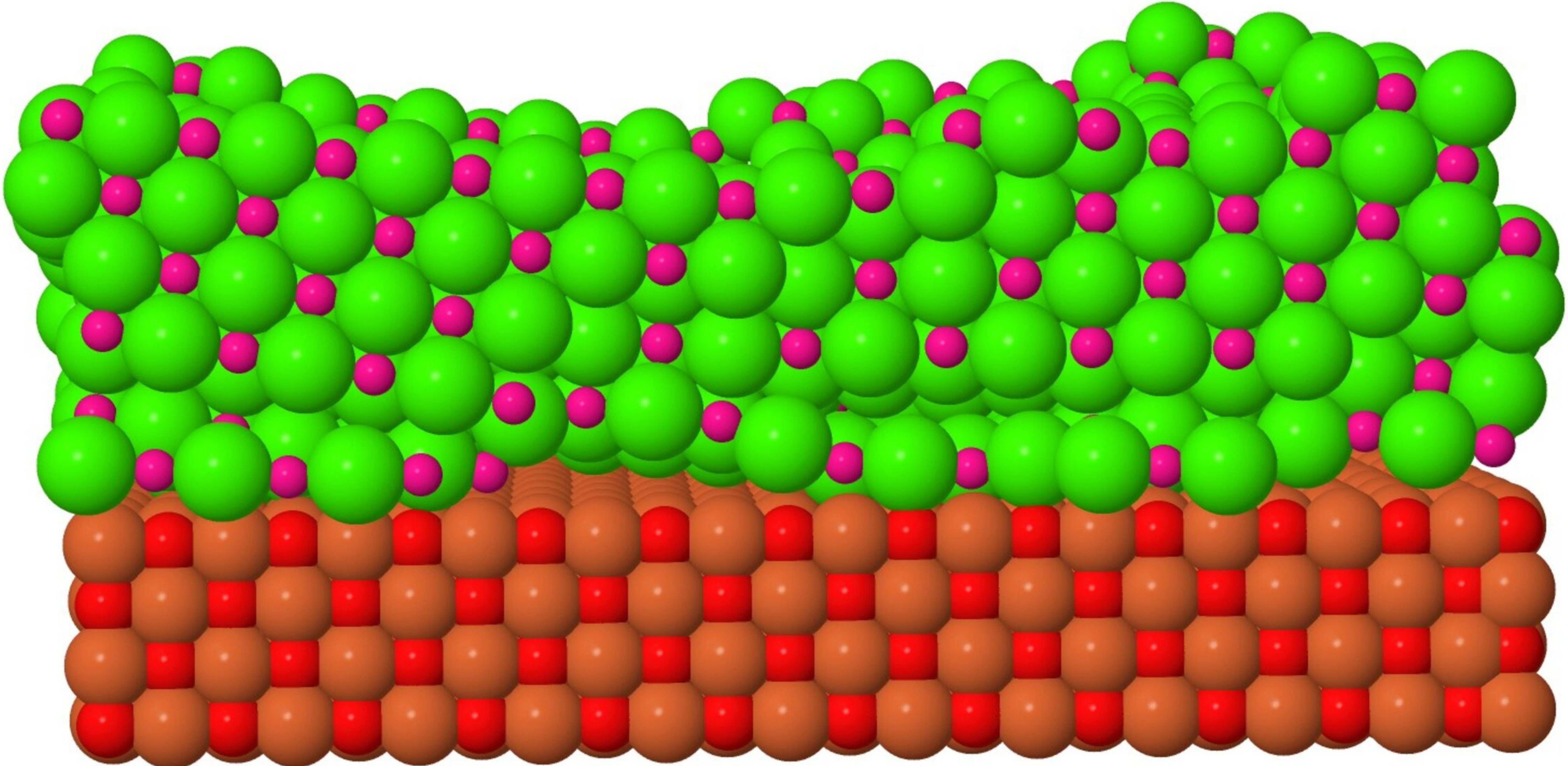g(r)
Ca-O_S
Ca-Ba
O_{TF}-Ba
O_{TF}-O_S
Ca-O_{TF}
O_{TF}-O_{TF}
0.0
0.2
0.4
0.6
0.8
1.0
1.2
1.4
1.6
1.8
2.0
2.2
2.4
2.6
2.8
3.0
0
10
20
30
40
50
60
70
80
1.0
1.5
2.0
2.5
3.0
3.5
4.0
4.5
5.0
5.5
6.0
distance (Å)